Revista GEOCIÊNCIAS

unesp

ISSN: 1980-900X (online)

POST-COLLISIONAL MAGMATIC EVOLUTION OF THE CASTELO INTRUSIVE COMPLEX, ESPÍRITO SANTO, BRAZIL: NEW U-Pb GEOCHRONOLOGICAL DATA AND INTEGRATION OF PETROGRAPHIC AND GEOCHEMISTRY EVIDENCE

EVOLUÇÃO MAGMÁTICA PÓS-COLISIONAL DO COMPLEXO INTRUSIVO CASTELO, ESPÍRITO SANTO, BRASIL: NOVOS DADOS GEOCRONOLÓGICOS U-Pb E INTEGRAÇÃO DE EVIDÊNCIAS PETROGRÁFICAS E GEOQUÍMICAS

Iago Mateus Lopes de MACÊDO[1], Mauro César GERALDES[1], Guilherme Loriato POTRATZ[1], Marilane Gonzaga de MELO[2], Rodson de Abreu MARQUES[3], Ana Paula MEYER[4], Renzo Dias RODRIGUES[1], Marcos Silva MACHADO [1], Armando Dias TAVARES[1]

[1]Universidade do Estado do Rio de Janeiro. Faculdade de Geologia, Avenida São Francisco Xavier, 524. Maracanã. Rio de Janeiro - RJ. E-mails: lopes.iago1@gmail.com; mauro.geraldes@gmail.com; geoloriato@gmail.com; renzodias10@hotmail.com; pardal.uerj@gmail.com; tavares.armandodias@gmail.com
[2]Universidade Federal do Espírito Santo. Departamento de Geologia. Rua Felício Alcure, 94-298 - Conceição, Alegre – ES. E-mail: marilanegonzaga@hotmail.com
[3]Universidade Federal de Ouro Preto. Morro do Cruzeiro, Bauxita. Ouro Preto – MG. E-mail: rodsonabreu@gmail.com
[4]Instituto Federal do Espírito Santo. Rodovia ES-482. Fazenda Morro Grande, Cachoeiro do Itapemirim – ES. E-mail: paulam@ifes.edu.br

ABSTRACT - The Castelo Intrusive Complex (CIC), located in the southern region of the Espírito Santos state, southeastern Brazil, is a pluton inserted in the context of post-collisional magmatism of the Araçuaí Orogeny, known as Supersuite G5, related to the extensional collapse during the Brasiliano/Pan-African Orogeny. This work integrates field, petrographic, lithogeochemical, and isotopic data, bringing new U-Pb ages for the CIC and a new geological map. The CIC presents a great compositional variety, presenting rocks of monzogranitic, granodioritic, quartz monzodioritic and dioritic. The U-Pb data from the granite from the northern edge, yielded an upper intercept age of 504 ± 6 My. The diorite from the massif's core yielded a 514 ± 6 My crystallization age. The granite from the western edge yielded a crystallization age of 529 ± 3 My. The U-Pb ages from the literature suggest two magmatic episodes (529-514 My and 510-504 My) for forming the CIC. The lithological variety of the CIC is also expressed in the lithogeochemical data set with a range of SiO_2 contents (50.19% to 74.14%) and in the variation observed in the R1-R2 diagram for the classification of plutonic rocks. The principal component analysis for lithogeochemical results reinforces the existence of two large groups of rocks, an older group 1 (granites, granodiorites, and tonalities) and a younger group 2 (granodiorites, mozodiorites, monzonites, diorites, and tonalites). The correlation matrices between the principal components reveal the prominent role of the magma mixing process. The normalized multi-element diagram of chondrite shows that the negative Eu anomaly was more pronounced for group 1 and enrichment in ETRL, with pronounced fractionation. The classification diagrams demonstrate that the rocks of the CIC are ferrous to weakly metaluminous, alkaline-calcic to calc-alkaline, with a positive trend between the silica content and the Na_2O+K_2O-CaO parameter, and meta- to peraluminous saturated in silica suggesting an alkaline arc environment for its origin.

Keywords: Zircon U-Pb ages. Pos-tectonic magmatism. Geochemistry. Araçuaí Orogeny.

RESUMO – O Complexo Intrusivo Castelo (CIC), localizado na região sul do estado do Espírito Santo, sudeste do Brasil, é um *plúton* inserido no contexto do magmatismo pós-colisional da Orogenia Araçuaí, conhecido como Supersuite G5, relacionado ao colapso extensional durante a Orogenia Brasiliano/Pan-Africana. Este trabalho integra dados de campo, petrográficos, litogeoquímicos e isotópicos, trazendo novas idades U-Pb para o CIC e um novo mapa geológico. O CIC apresenta uma grande variedade composicional de rochas monzogranítica, granodiorítica, quartzo monzodiorítica e diorítica. Os dados U-Pb do granito da borda norte produziram uma idade com interceptação superior de 504 ± 6 Ma. O diorito do núcleo do maciço rendeu uma idade de cristalização de 514 ± 6 Ma. O granito da borda oeste produziu uma idade de cristalização de 529 ± 3 Ma. As idades U-Pb da literatura sugerem dois episódios magmáticos (529-514Ma e 510-504 Ma) para a formação do CIC. A variedade litológica do CIC também é expressa no conjunto de dados litogeoquímicos com uma faixa de teores de SiO_2 (50,19% a 74,14%) observada na variação no diagrama R1-R2 para a classificação de rochas plutônicas. A análise de componentes principais para resultados litogeoquímicos reforça a existência de dois grandes grupos de rochas, um grupo 1 mais antigo (granitos, granodioritos e tonalidades) e um grupo 2 mais jovem (granodioritos, monzodioritos, monzonitos, dioritos e tonalitos). As matrizes de correlação entre os componentes principais revelam o papel proeminente do processo de mistura do magma. O diagrama multielementos normalizado pelo condrito mostra que a anomalia negativa de Eu foi mais pronunciada para o grupo 1 e o enriquecimento em ETRL, com fracionamento pronunciado. Os diagramas de classificação demonstram que as rochas do CIC são ferrosas a fracamente metaluminosas, alcalino-cálcico a cálcio-alcalina, com tendência positiva entre o teor de sílica e o parâmetro Na_2O+K_2O-CaO, e meta- a peraluminosa saturada em sílica sugerindo um ambiente alcalino de arco para sua origem.

Palavras-chave – Idades U-Pb em zircão. Magmatismo pós-tectônico. Geoquímica. Orogenia Araçuaí.

INTRODUCTION

The period of continental collision is marked by intense metamorphism, melting, and continental growth due to crustal accretion (Song et al., 2015; Bonin et al., 2004). Following this period, there is the post-collisional stage, where mafic magmas of mantle origin access the felsic continental crust and can mix, generating different products due to the degree of hybridization and being observed both at the outcrop scale and in thin sections (Liégeois et al., 1998, Sklyarov & Fedorovskii, 2006; Perugini et al., 2010; Sami et al., 2018). Many authors consider the mixing process as the primary mechanism capable of generating compositional variations in suites of igneous rocks (Perugini et al., 2013; De Campos, 2015; Wang et al., 2022).

Although many authors oppose the mixing process due to the physical difficulties involving contrasting magmas in terms of temperature, viscosity, and degree of crystallinity, among other parameters, the diffusion capacity of the elements allows the mixing mechanism to occur, leading to degrees of homogenization that can be modeled from a geochemical point of view through numerical simulations and experiments (Perugini et al., 2013; De Campos, 2015). In addition, zircon can be used as a powerful petrogenetic tool to trace magma sources (Gagnevin et al., 2010; Yang et al., 2007).

The Araçuaí Orogeny, located in southeastern Brazil and involving the states of Espírito Santo and Minas Gerais, records a long evolutionary history marked by different stages of collision, metamorphism, and magmatism. Intense magmatic activity between 530 and 480 My (Pedrosa-Soares et al., 2011, 2020) marks the post-collisional stage. The age itself cannot mark the post-collisional nature of the intrusive complex. There should be a fact that the regional tectonic frame favors this tectonic setting with the support of field data, and the results here reported aim to contribute to constraining the source and the magmatic processes.

The rocks generated during this period present a broad compositional spectrum, ranging from gabbro/norite to syenogranite, and several features related to magma mixing (De Campos et al., 2016). The Castelo Intrusive Complex (CIC) is a representative of the post-collisional suite, presenting a wide compositional variation ranging from monzogranite to diorite and exhibiting several features related to magma mixing. Some of its units have recently been studied from a geochronological and isotopic point of view (Macedo et al., 2022).

This work aims to understand the petrogenetic process involved in the formation of the complex, unraveling the magma sources. In this we present the new facies map for the intrusive complex, detail the petrographic characteristics of the rocks that compose it, and present new chemical and geochronological data (U-Pb). The literature presents a comprehensive study of G5 supersuite magmatism across a vast temporal range (500 My granites). Still, the studies focus on a relatively small dataset and limited U-Pb age constraints. Post-collisional suites present a limited integration comparing size and extent to other plutons in the same supersuite.

We selected CIC because magmatic processes are unique and do not align with regional descriptions of other bodies. We present a contextualization discussion with other well-studied post-collisional complexes in Araçuaí Orogeny to provide a more robust framework for understanding the significance of the CIC within the broader tectonic evolution.

GEOLOGICAL SETTING

The Araçuaí Orogeny, together with the Western Congo Orogeny, constitutes an orogenic system developed in the embayment of the São Francisco and Congo paleocontinents during the Brasiliano-Pan-African event, which extended from the Neoproterozoic to the Cambrian-Ordovician boundary. The collision resulted in the closure of the Adamastor Ocean and the consolidation of the West Gondwana supercontinent (Figure 1) (Alkmim et al., 2006, 2017). The Araçuaí-Western Congo Orogeny remained amalgamated until the opening of the South Atlantic Ocean in the Cretaceous (Tedeschi et al., 2016; Pedrosa-Soares et al., 2020).

Located in the northern portion of the Mantiqueira Province, the Araçuaí Orogeny is bordered to the north and west by the São Francisco Craton, to the east by the Atlantic Margin, and to the south by the Ribeira Orogeny (Almeida et al., 2000; Heilbron et al., 2004). The boundary of the Araçuaí and Ribeira Orogens has been the target of several studies to connect them since no marked discontinuity is observed between them. Instead, a certain continuity is observed between

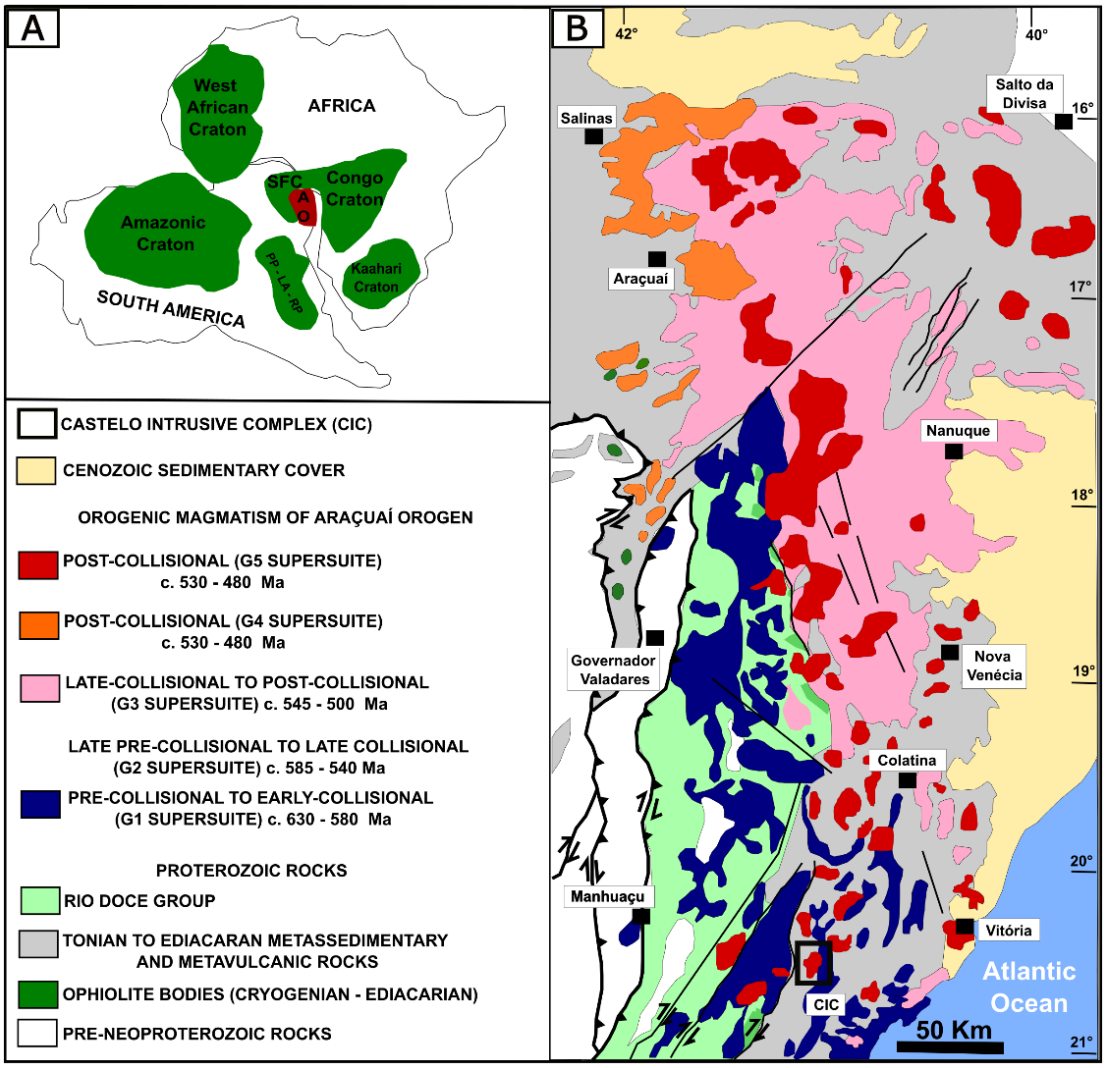

Figure 1 - (1A) Representation of the West Gondwana Supercontinent, delimiting the Araçuaí Orogeny and the adjacent cratonic regions (Modified from Alkmim et al., 2006). (1B) Simplified geological map of the Araçuaí Orogeny (Modified from Pedrosa-Soares et al., 2011), showing the study area black rectangle).

the rocks that compose them, mainly the magmatic arcs, thus forming the Araçuaí-Ribeira Orogenic System (AROS) (Degler et al., 2018; Corrales et al., 2020; Heilbron et al., 2020; Santiago et al., 2022).

Alkmim et al. (2006) proposed an evolution model for the Araçuaí Orogeny known as "nutcrack-er," divided into five stages: 1) Formation of the precursor Macaúbas basin, 2) Initial convergence stage, 3) Collisional stage, 4) Lateral escape stage of the southern portion, and 5) Gravitational collapse of the Orogeny. Based on fieldwork, structural, petrographic, geochemical, geochronological, and isotopic data, Pedrosa-Soares et al. (2011, 2020) grouped the magmatism of the Araçuaí Orogeny into five supersuites, reflecting different stages of the evolution, known as: G1 (630–580 My), G2 (585–540 My), G3 (545–500 My), G4 and G5 (530–480 My), the last two suites are in the same range of ages, but are formed in different sources (mantelic and crustal, respectively).

Supersuite G1 corresponds to the pre-collisional stage, comprising the plutonic arc section. It consists of an expanded calc-alkaline-magnesian series, formed essentially by rocks of granodioritic to tonalitic composition, in addition to mafic enclaves of dioritic composition (Gradim et al., 2014; Gonçalves et al., 2014, 2016, 2018; Tedeschi et al., 2016; Richter et al., 2016; Pedrosa-Soares et al., 2020; Santiago et al., 2020; Soares et al., 2020). The supracrustal sequences related to the arc are formed by metavolcanic - sedimentary successions, corresponding to the Rio Doce Group and other related basins, such as the Nova Venécia and Paraíba do Sul Complexes (Gradim et al., 2014; Richter et al., 2016). Supersuite G2 comprises the syn-collisional stage and is composed of S-type granitoids, sub-alkaline to alkaline and peraluminous, while supersuite G3 represents the late collisional stage (Gradim et al., 2014; Peixoto et al., 2015; Richter et al., 2016;

Melo et al., 2017a, b; Santiago et al., 2023). The post-collisional stage is represented by two super suites, G4 and G5, which consist of calc-alkaline to alkaline granitoids, free from regional deformation (De Campos et al., 2016; Pedrosa-Soares et al., 2011).

G5 supersuite

Several intrusive bodies mark the post-collisional magmatism of the Araçuaí Orogeny with elliptical, concentric, and oval shapes related to the gravitational collapse of the orogen. These plutons typically have gabbroic/noritic cores surrounded by syenites, monzonites, and granites and may have external rings of norite and charnockite (Pedrosa-Soares et al., 2001 2011; Wiedemann-Leonardos et al., 2002; De Campos et al., 2016).

The most striking characteristics of these plutons are the absence of regional foliation, evidence of magmatic flow and features related to magma mixing, such as net-veined granitic intrusions, micro granular mafic enclaves and schlieren like features in granites (Bayer et al., 1987; Schimidt-Thomé & Weber-Diefenbach. 1987; Medeiros et al., 2001; Mendes et al., 2005; Mendes & De Campos, 2012; Aranda et al., 2020; Araújo et al., 2020; Duffles Teixeira et al., 2020; Melo et al., 2020; Bellon et al., 2022; Macedo et al., 2022; Potratz et al., 2022).

These plutons intrude pre- and syn-collisional granitoids and paragneisses (Nova Venécia Complex, Paraíba do Sul, Jequitinhonha). Geothermobarometric data indicate emplacement at shallow to intermediate crustal levels, showing for the plutons in the southern region of Espírito Santo, such as Pedra Azul, Afonso Cláudio, Santa Angélica, Mimoso do Sul, Venda Nova and Castelo, crystallization at pressures of 5.7 to 11.5 kbar, while the plutons located in the north of the state of Espírito Santo and northeast of Minas Gerais, such as Várzea Alegre, Pedra do Elefante, Barra de São Francisco, Padre Paraíso and Medina, present crystallization at pressures of 2.4 to 3.5 kbar (Sollner et al., 2000; Martins et al., 2004; Petitgirard et al., 2009; Baltazar et al., 2010).

The G5 supersuite magmatism (Figure 2), which corresponds to the last regional event recorded in the Araçuaí Orogeny, is an important tectonic marker due multiple magmatic processes and sources. This magmatism was triggered by the rise of a hot asthenospheric mantle related to the slab break-off during subduction, followed by a delamination process favoring the crustal anatexis. Isotopic data show a considerable variation for the ratios $^{87}Sr/^{86}Sr$ (0.702–0.741), $\varepsilon_{Nd(t)}$ (- 3 to - 24), Nd T_{DM} (1.4–2.6 Gy), $\varepsilon_{Hf(t)}$ (+12 to - 24), and Hf T_{DM} ages (1.25–2.4 Gy). Zircon U-Pb ages for the plutons show an age range of 530 to 480 My (Aranda et al., 2020; Araújo et al., 2020; Bellon et al., 2022; Potratz et al., 2022).

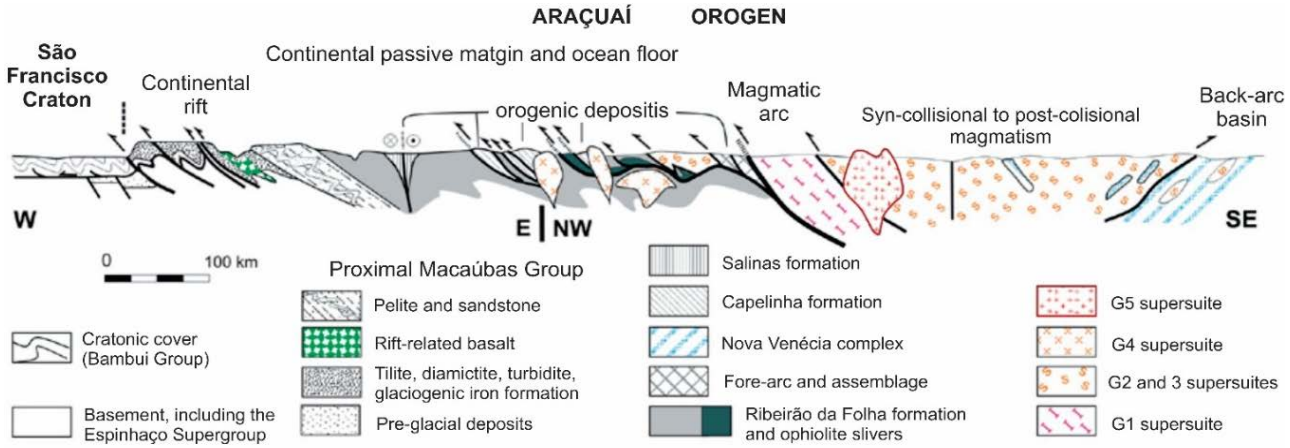

Figure 2 – Schematic profile of the Araçuaí-Western Congo Orogen, focusing on the Neoproterozoic portion. The schematic profile of the Araçuaí-Western Congo Orogen is highlighted here only in the domains that correspond to the Brazilian portion of this orogen. Adapted from Pedrosa-Soares et al. (2001).

MATERIALS AND METHODS

Fieldwork in the Castelo Intrusive Complex was conducted between 2019 and 2022 with the host rocks were identified, twenty-eight samples (from the intrusive complex) were collected to prepare thin sections and three samples for U-Pb geochronology in zircon grains. The samples for geochronology were prepared at the Geological Sample Preparation Laboratory (LGPA) of the State University of Rio de Janeiro (UERJ). The samples were then washed, manually reduced using a sledgehammer and anvil, crushed (jaw crusher), and powered (disc mill). The pulverized

material underwent density separation processes, starting with the hydrodynamic separation table and followed by separation using dense liquids (iodide and bromoform).

Finally, the concentrates underwent magnetic separation (Franz) and manual sorting. After epoxy preparation (fixation of zircon grains to an epoxy resin), the samples are sent to the polishing process of the mount for subsequent imaging in a QUANTA 250 Scanning Electron Microscope (SEM) to produce backscattered and cathodoluminescent images. The SEM image of the zircon grains allows observation of the internal structure of the mineral and evidence of inherited core, areas of reabsorption, and magmatic zoning to guide the subsequent location of the isotopic analysis.

The U-Pb analyses on zircon grains were performed at the Multiuser Environmental Laboratory (MultiLab) – UERJ, using a Laser-Induced Plasma Mass Spectrometer (LA-ICP-MS) through the Element-2 equipment. The order of data reading in the equipment was: (1) blank reading, (2) reading of the GJ-1 standard, (3) reading of the GJ-1 standard, (4) reading of the 91500 standards, (5) reading of eighteen unknown grains, (6) reading of the blank (Jackson et al., 2004). The complete description of the sample preparation at MultiLab (UERJ-Brazil) is reported by Alves et al. (2019).

The grain surface was ablated using laser pulses with a diameter of 30 μm. The material vaporized by the laser (excimer 193μm) was transported in Ar (0.80 L/min) and He (0.55 L/min) for analysis using 700 cycles of 1 second each. The analyses included mass measurements of ^{204}Pb, ^{206}Pb, ^{207}Pb, 208Pb, ^{232}Th and ^{238}U. Hg contaminant in He and Ar gases was corrected, due to the isobaric ^{204}Hg interference with the ^{204}Pb mass. The samples were analyzed together with the zircon reference materials GJ-1 (TIMS normalization data ^{207}Pb/^{206}Pb = 608.3 My, ^{206}Pb/^{238}U = 600.7 My and ^{207}Pb/^{235}U = 602.2 My (Alves et al., 2019) and the results obtained during this investigation was 608.5 ± 0.4My. For reference material 91,500 (TIMS-ID age for ^{206}Pb/^{238}U = 1062.4 ± 0.8 My and ^{207}Pb/^{206}Pb = 1065.4 ± 0.6 My, according to (Alves et al., 2019), and the results obtained here indicate a crystallization age of 1065 ± 6 My.

The thin sections were analyzed by an ocular microscope before the selection of samples for geochemistry. The chemical analyses were performed at Acme Analytical Laboratories Ltda (Vancouver). The samples analyzed in the ICP-ES were digested by fusion of lithium metaborate/tetraborate and dilute nitric acid, requiring 0.2 g of each sample. The ICP-ES was used to measure SiO_2, Al_2O_3, Fe_2O_3, MgO, CaO, Na_2O, K_2O, TiO_2, P_2O_5, MnO, Cr_2O_3, Ni, Sc. The analyses of Ba, Be, Co, Cs, Ga, Hb, Nb, Sn, Sr, Ta, Th, U, V, W, Zr, Y, and rare earth elements (REE) were obtained using ICP-MS, with samples fusion obtained by lithium metaborate/ tetraborate and digestion in nitric acid, requiring 0.2 g of each sample. For the analyses of Mo, Cu, Pb, Zn, Ni, As, Cd, Sb, Bi, Ag, Au, Hg, Tl, and Se, also performed by ICP-MS, 0.5 g of each sample and digestion in aqua regia were required.

Each batch of samples analyzed contains a blank method reagent, certified reference materials, and 6% replicates. Analyses were performed using a Perkin Elmer Sciex ELAN 6000, 6100, or 9000 ICP-MS. A set of 10 certified reference materials was run before and after each batch of samples. Duplicates were analyzed after every 17 samples, and the instrument was calibrated after every 2 sample trays. Data was processed and analyzed using Microsoft Excel and Geochemical Data Toolkit (GCDkit) version 6.0.5.

RESULTS

Field description and petrography

The Castelo Intrusive Complex (Figure 3) generally has an elliptical shape and mountainous relief. However, it has some lowered portions in the southern and central regions of the massif. Outcrops are observed in road cuts, quarries, walls, and waterfalls. Blocks and boulders are common and are associated with the exploitation of dimension stones in quarries. The boundary between the pluton and its host rocks is well-marked by geomorphology.

The mapped units in the Castelo Intrusive Complex are (i) Porphyritic monzogranite, (ii) Fine to coarse inequigranular monzogranite, (iii) Granodiorite, (iv) Quartz monzodiorite, and (v) Diorite (Figure 4) (Table 1). The CIC has a steep sub-vertical escaped relief, forming elongated mountain ranges with rounded tops, mainly in the granite domain outside this domain, where granodiorite, diorite, and quartz-monzodiorite outcrop, and the relief tends to be lower, where the main drainages are located.

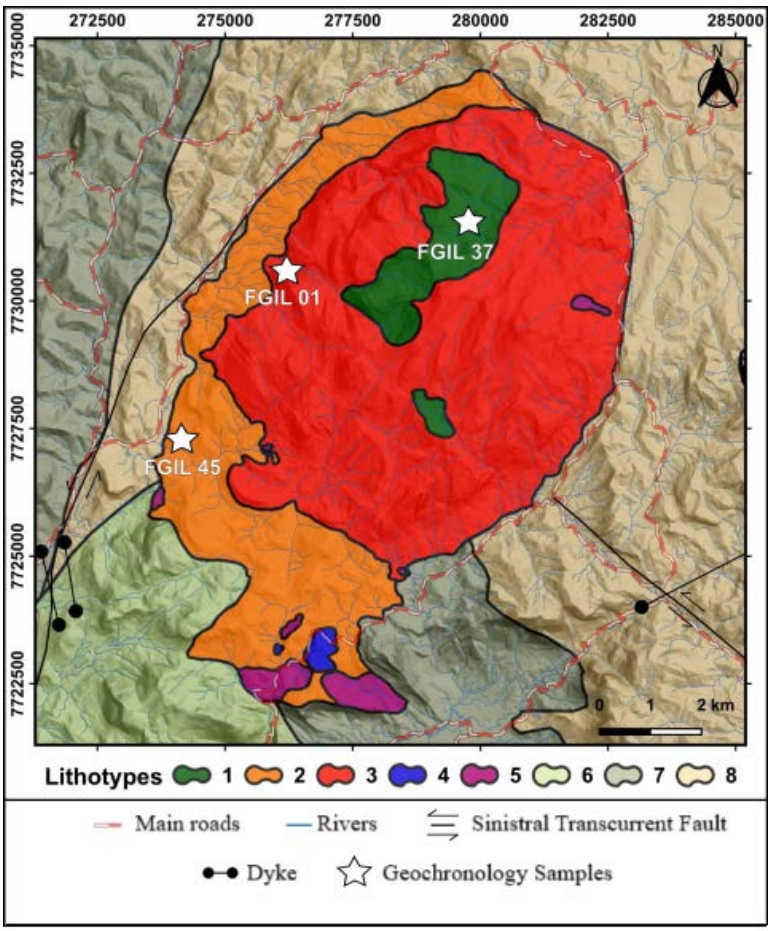

Figure 3 - CIC geological map. (1) Diorite; (2) Fine- to coarse-grained inequigranular monzogranite; (3) Porphyritic monzogranite; (4) Granodiorite; (5) Quartz monzodiorite; (6) São Fidelis paragneisses; (7) Italva paragneisses; (8) Orthogneiss.

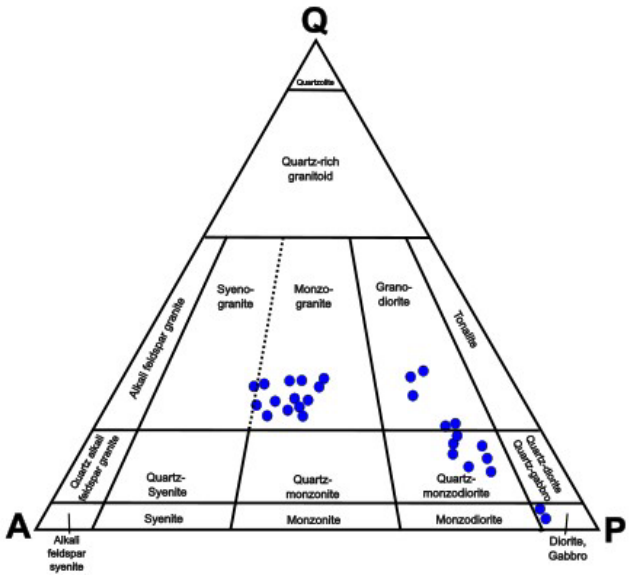

Figure 4 - QAP diagram for the rocks of the Castelo Intrusive Complex (Modified from Streckeisen, 1976).

Table 1 - Mineralogical description of all rock types in this study, using the mineral abbreviations of Whitney & Evans (2010).

Rock Type	Main Mineralogy	Accessory Mineralogy
Monzogranite	Qtz + Kfs + Pl + Bt	Opq + Ttn + Ap + Zrn + Aln + Hbl
Granodiorite	Qtz + Kfs +Pl + Bt + Hbl	Opq + Ttn + Ap + Zrn
Quartz monzodiorite	Qtz + Kfs + Pl + B t+ Hbl	Opq + Ttn + Ap
Diorite	Pl + Bt + Hbl	Qtz + Kfs + Opq + Ttn+ Ap + Zrn
Mafic dikes	Pl + Opq	Tin + Ap

The topographic contrast between the host rocks and the CIC is that the host rocks are usually presented as gentler mountain ranges, hills, and mountains.

The host rocks of the CIC are (i) biotite gneiss with amphibolite enclaves, (ii) migmatitic paragneiss, and (iii) marble with amphibolite intrusions. Biotite gneiss is the main unit hosting the CIC. It presents discontinuous metamorphic banding, sometimes continuous, spaced millimetrically to centimetrically, consistent with the regional foliation, marked mainly by K-feldspar porphyroblasts in the felsic band and by biotite and amphibole in the mafic band.

The migmatitic paragneiss unit presents a gradational contact with the biotite gneiss unit, and its principal characteristic is the features related to migmatization. Marble with amphibolite intrusions occurs in isolated lenses with exploration queries. The main characteristics of this unit are the skarnitization processes and structures, such as concentric folds and boudins.

The monzogranite outcrops are mainly at the edges of the massif (Figure 5A), presenting only facies variation without compositional change. The edge of the Castelo Intrusive Complex is marked mainly by the fine- to coarse-grained inequigranular monzogranite (Figure 5B), passing to the porphyritic monzogranite, with K-feldspar phenocrysts of up to 6 cm (Figure 5C), as it approaches the center of the intrusion. These two facies present micro granular mafic enclaves (Figure 5D) of different compositions, sizes, and textures, and features analogous to schlieren of various sizes and sometimes oriented.

Mafic dikes are observed occasionally, and syn plutonic mafic dikes with a high degree of hybridization with the host granite are common. Pegmatitic dikes and intrusions of late leucogranites and even mafic rocks are common, generating agmatic features (Figure 5E). Xenoliths of the host rock are observed in both facies, presenting various sizes and shapes and degrees of assimilation. In the porphyritic facies, the alignment of K-feldspar phenocrysts is joint, indicating igneous flow.

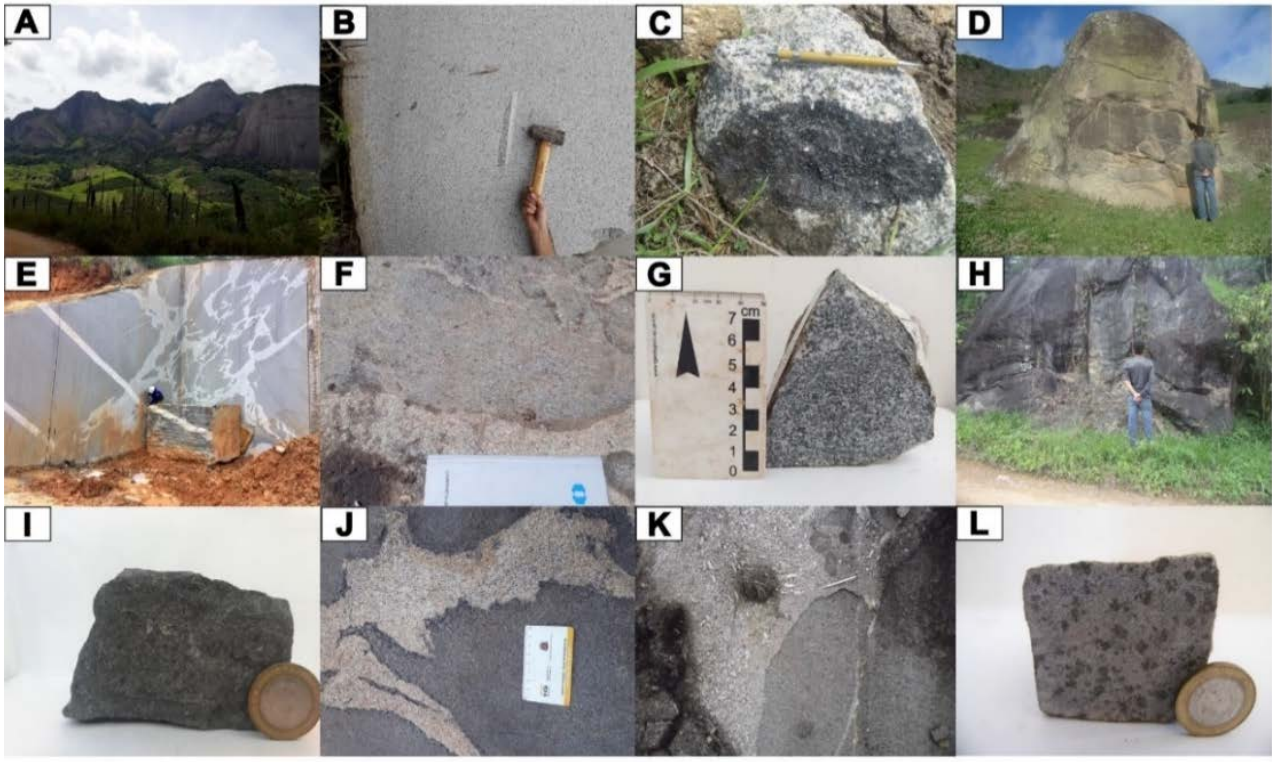

Figure 5 - A) Topographic contrast between the hills of the country rocks and the steep relief of the CIC, B) Quarry cut of the fine-grained monzogranitic facies, C) Microgranular mafic enclave present in the porphyritic monzogranite, D) Large micro granular mafic enclave in a block of porphyritic monzogranite, E) Agmatic feature observed in a quarry cut at the edge of the CIC, F) Granodiorite outcrop with late granitic intrusion, G) Granodiorite hand sample, H) Quartz monzodiorite outcrop in the south-central portion of the CIC, I) Quartz monzodiorite hand sample, J) Quartz monzodiorite outcrop with granitic intrusion forming cooled margins and hybrid zones, K) Diorite outcrop in the central portion of the CIC, showing granitic intrusions, L) Hand species of diorite.

The composition of the monzogranite (Figure 6A to D) of: Microcline (40-30%), orthoclase (15-20%), plagioclase (30-20%), quartz (35-25%), biotite (25-15%), titanite (5%), opaques minerals (5%), allanite (2-5%), zircon (1%), hornblende (<1%). Muscovite (<1%), sericite

(<1%), chlorite (<1%) and carbonates (<1%) are secondary minerals.

Granodiorite is the least common lithotype, occurring punctually in the central-southern portion of the CIC. It is usually gray and often yellowish, with an inequigranular texture and fine to medium grain size (Figure 6E). It presents small plagioclase xenocrysts, mostly rounded and mafic enclaves. It is common to observe clots of mafic minerals and leucocratic injections of granite in the form of dikes or pockets (Figure 6F). When the grain size is fine, it usually presents a salt and pepper texture due to the contrast in color between the felsic and mafic minerals.

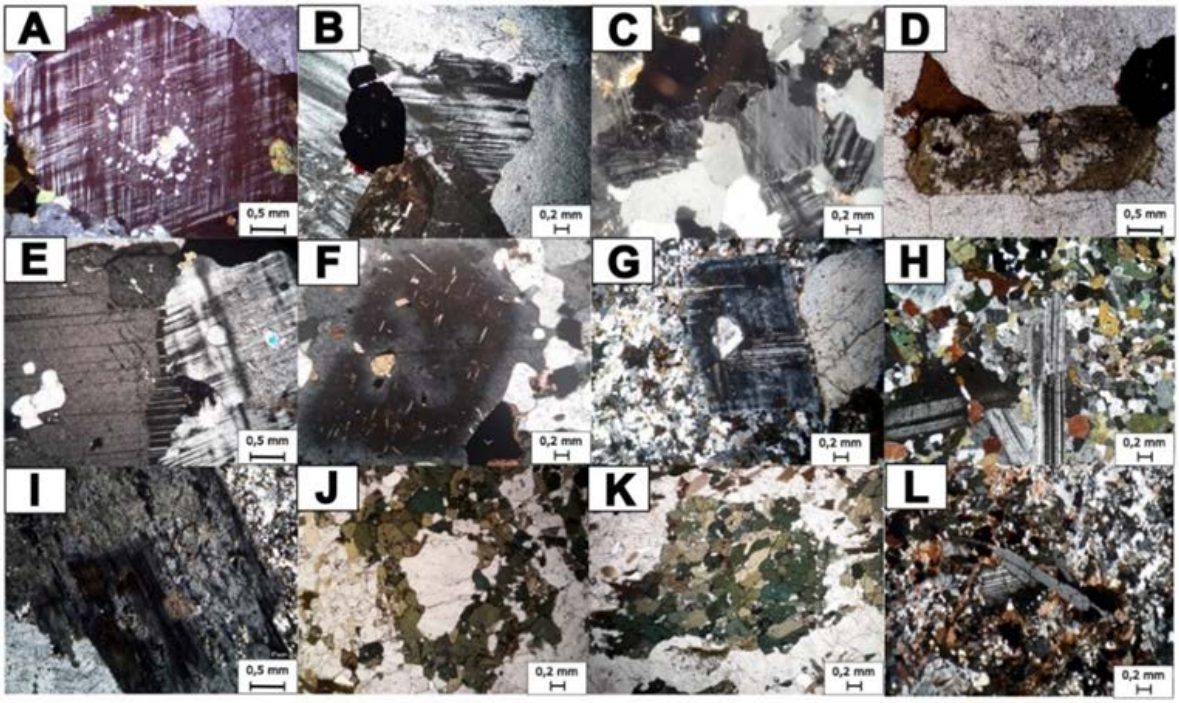

Figure 6 - A) Poikilitic microcline crystal in monzogranite; B) K-feldspar in monzogranite; C) Quartz and microcline crystals in monzogranite; D) Allanite crystal in monzogranite; E) Syntax texture in plagioclase crystal in granodiorite; F) Zoned plagioclase crystal in granodiorite; G) Zoned plagioclase crystal in quartz monzodiorite; H) Plagioclase lath with corrosion edges in quartz monzodiorite; I) Plagioclase crystal showing boxy cellular texture in quartz monzodiorite; J) Ocellar quartz-hornblende texture in diorite; K) Mafic mineral clots in diorite; L) Mix of apatite crystals in diorite.

The mineralogy consists of: Quartz (35-25%), plagioclase (35-25%), orthoclase (10-15%), biotite (15-25%), hornblende (15-20%), titanite (5%), opaque minerals (5%), apatite (1-5%), zircon (<1%). Sericite (1%) and chlorite (1%) are secondary minerals. It presents plagioclase crystals evidencing compositional zoning (Figure 6E, F).

Quartz monzodiorite is the predominant unit in the mixed zone, often associated with monzogranite, in contact with it, and is predominant in the central-southern portion of the CIC (Figure 5H). It is dark gray to black in color, meso- to melanocratic, equigranular, and fine-grained (Figure 5I). Coarse-grained granitic intrusions in the form of veins, pegmatites, and pockets are widespread in interdigitated to abrupt contacts (Figure 5J). From the interaction between the host quartz monzodiorite and the granitic intrusions, some features related to magma mixing are found, such as chilled margins, features analogous to pillows, rounded, corroded feldspar xenocrysts, and zones of inclusion of mafic minerals in these xenocrysts, in addition to small mixing zones.

The mineralogy consists of plagioclase (40-30%), hornblende (30-20%), biotite (20-10%), quartz (10%), orthoclase (10%), titanite (5%), and opaque minerals and apatite (<5%). From a microscopic point of view, this lithotype presents features indicative of mixing, recorded mainly in the plagioclase, such as compositional zoning (Figure 6G), plagioclase laths with evidence of corrosion at the edges (Figure 6 H), boxy cellular textures (Figure 5I) and slots of mafic minerals. Other textures related to magma mixing are apatite crystal mix and poikilitic texture.

Diorite occurs in the core of the CIC, in the topographically lowest region, surrounded by large monzogranite scarps and appearing as large enclaves within them. Several coarse-grained granite dikes and pockets with tabular K-feldspar phenocrysts (Figure 5K) were cut. The diorite is dark gray in color, melanocratic, equigranular, medium to coarse-grained, and has mafic clots of

a few centimeters (~ 3 cm) (Figure 5L).
Its composition consists of hornblende (40-35%), plagioclase (35-30%), biotite (25-20%), quartz (8-5%), orthoclase (5%), apatite (5%), opaques minerals (5%), titanite (5%), and zircon (1%). Biotite, hornblende, and apatite aggregates are common, in addition to quartz xenocrysts, which in some cases are surrounded by hornblende crystals, evidencing the ocellar quartz-hornblende texture (Figure 6J, K, L).

Lithogeochemical results

New lithogeochemical results (18 samples) are presented in supplementary material A. The lithogeochemical data presented here were compiled from De Campos et al. (2004) (13 samples), Medeiros (2013) (6 samples), and Meyer (2017) (11 samples).

Each of the works presents different lithological classifications for the rocks of the CIC. Therefore, we grouped the rocks regarding chemical classification, as observed in the classification diagram R1-R2 (Figure 7), adapted from (De La Roche et al., 1980). The new types of rocks obtained by the chemical classification are not representative of being included in the map (Figure 3).

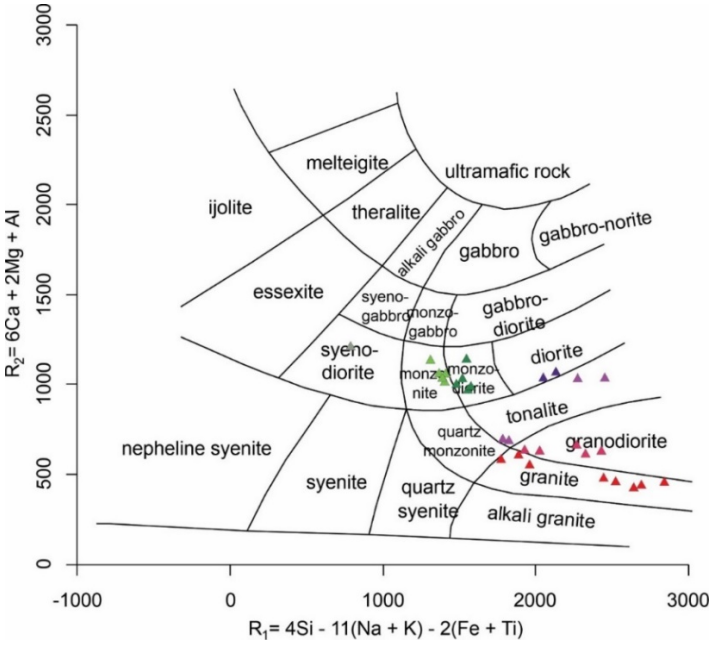

Figure 7 - Diagram R1-R2, adapted from (De La Roche et al., 1980) for the classification of plutonic rocks, where lithogeochemical data of the rocks of the Castelo Intrusive Complex are plotted. The samples symbols are presented in figure 8 legend.

The chemical classification diagram (Figure 8) demonstrates the compositional variation of the rocks of the CIC, where syenodiorite, monzodiorite, monzonite, diorite, tonalite, granodiorite, and granite are present. The SiO_2 content demonstrates the compositional variability of the rocks of the CIC, ranging between 50.19 and 74.14% (Figure 8). Figure 8 shows the behavior of the main oxides concerning the variation in the SiO_2 content, where a possible "compositional gap" (3.72%) was observed between 58.17% and 61.89% of SiO_2.

Figure 9 presents the principal component analysis performed with the main oxides (Figure 9A) and the trace elements (Figure 9B) available in the compiled works. The possible compositional gap demonstrated in the Harker diagrams delimits two large sets of rocks in the CIC, and this same pattern is observed in the principal component analysis (Figure 8A).

The group composed of granites, granodiorites, and two tonalite samples (group 1) is strongly influenced by the SiO_2 and K_2O vectors, where the low angle between the vectors demonstrates their high correlation.

The second group, composed of syenodiorite, monzodiorite, monzonite, diorite, and two tonalite samples (group 2), is strongly influenced by the vectors CaO, TiO_2, Fe_2O_3, MnO, P_2O_5, and MgO, where the CaO-TiO_2, Fe_2O_3-MnO and P_2O_5-MgO pairs are highly correlated.

The principal component analysis for the trace elements demonstrated that group 1 can be subdivided into two groups (Figure 9B). The behavior of Rb strongly influences one subgroup, with some influence of Ga, and the other subgroup is influenced by the behavior of Zr. Subgroup 2 presents a more dispersed pattern (Figure 8B). However, a set of samples is strongly influenced by Ba and Nb.

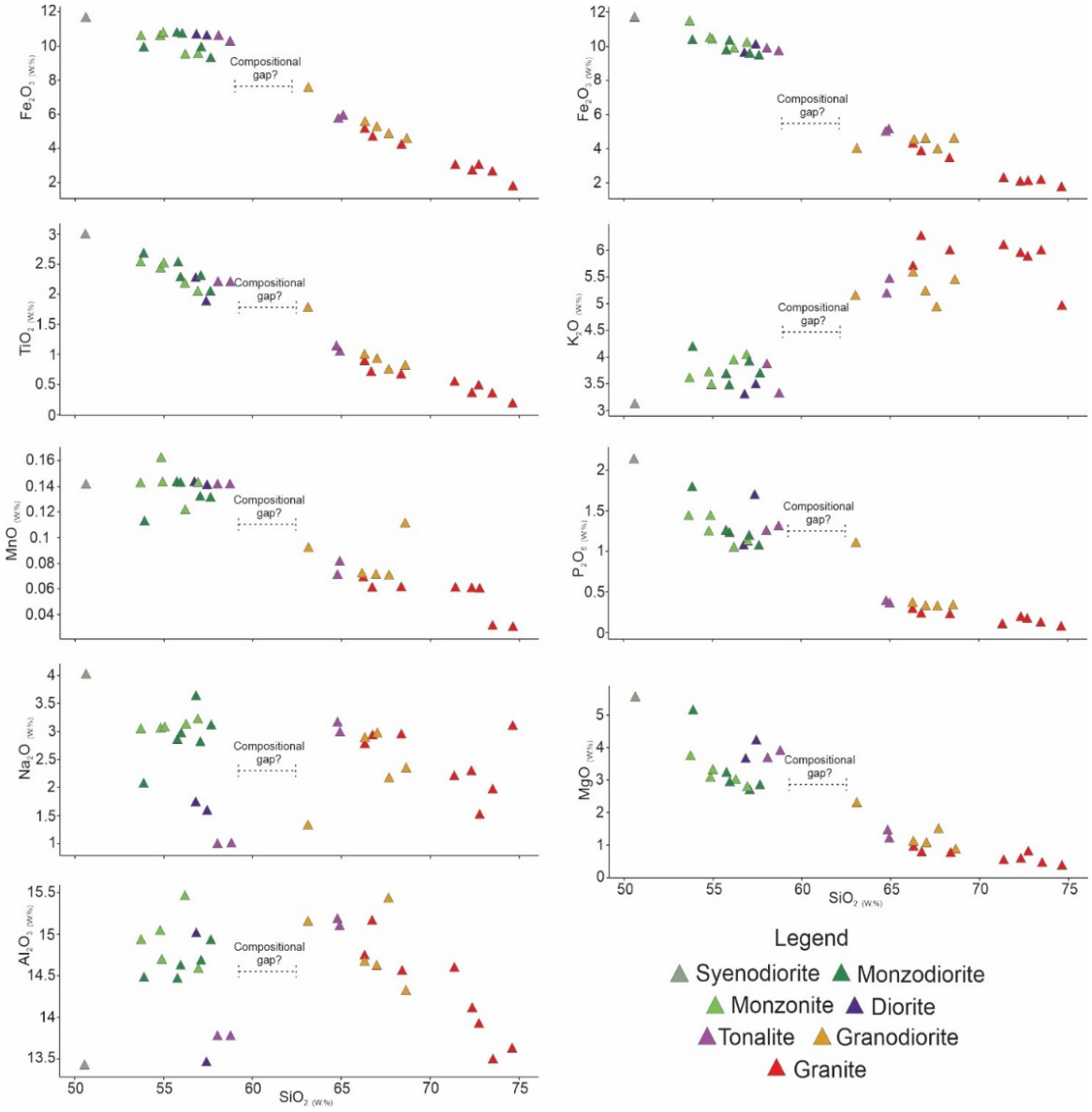

Figure 8 - Main oxides versus silic content (Harker) diagrams for the CIC samples, showing two groups with distinct characteristics separated by a compositional gap. The samples symbols are presented in Figure 8 legend.

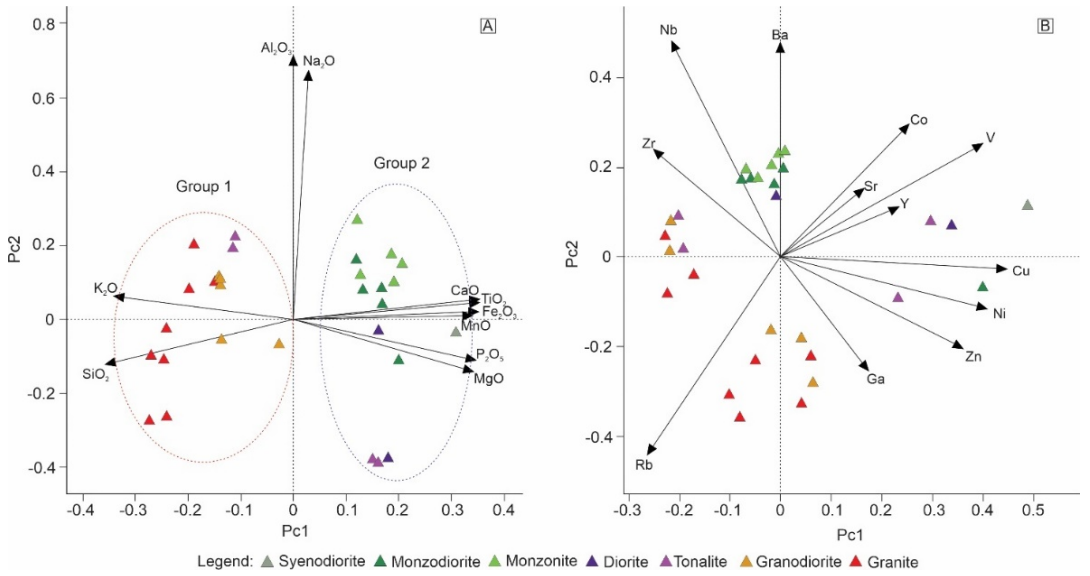

Figure 9 - A) Principal component analysis for the major elements (SiO_2, Al_2O_3, Fe_2O_3, CaO, MgO, MnO, Na_2O, K_2O, TiO_2, P_2O_5) indicating two distinct groups for the CIC rocks. B) Principal component analysis for the trace elements indicating subdivision of group 1 and dispersed pattern of group 2. The samples symbols are presented in figure 8 legend.

Correlation matrices were calculated for the two large groups observed in the principal component analysis. Molar ratios were calculated for each oxide to standardize the elements, converted from % by weight to parts per million (ppm). In figure 10, the color bar is associated with different r2 values. The r2 values are generally low to intermediate for both groups, except for the Fe-Si and Fe-Ti pairs in group 1, where the r2 values are more significant than 0.8 (Figure 10).

In the multielement diagram with samples normalized to the chondrite (Boynton, 1984) (Figure 11), the set of rocks from group 1 shows a more significant negative anomaly in Eu than the samples from group 2. Both groups were observed to present pronounced LREE enrichment to LREE.

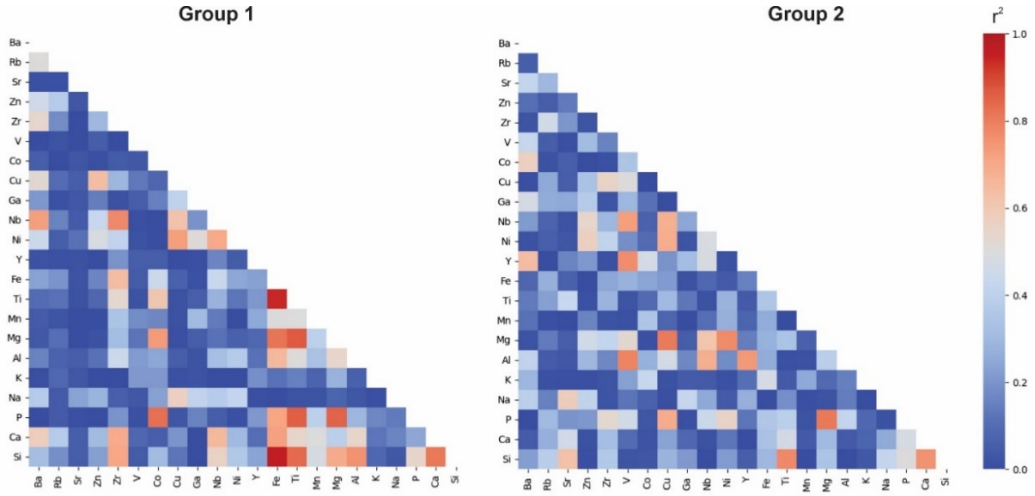

Figure 10 - Correlation matrices for major and trace elements in the Castelo Intrusive Complex's geochemical groups 1 and 2. The color bar on the right indicates the colors associated with different r2 values.

In the multielement diagram with samples normalized to the primitive mantle (Sun and McDonough, 1989) (Figure 11), the set of rocks from group 2 presents negative anomalies for Ti, Zr, Sr, and Nb and enrichment for Ba, Th, La, and Nd.

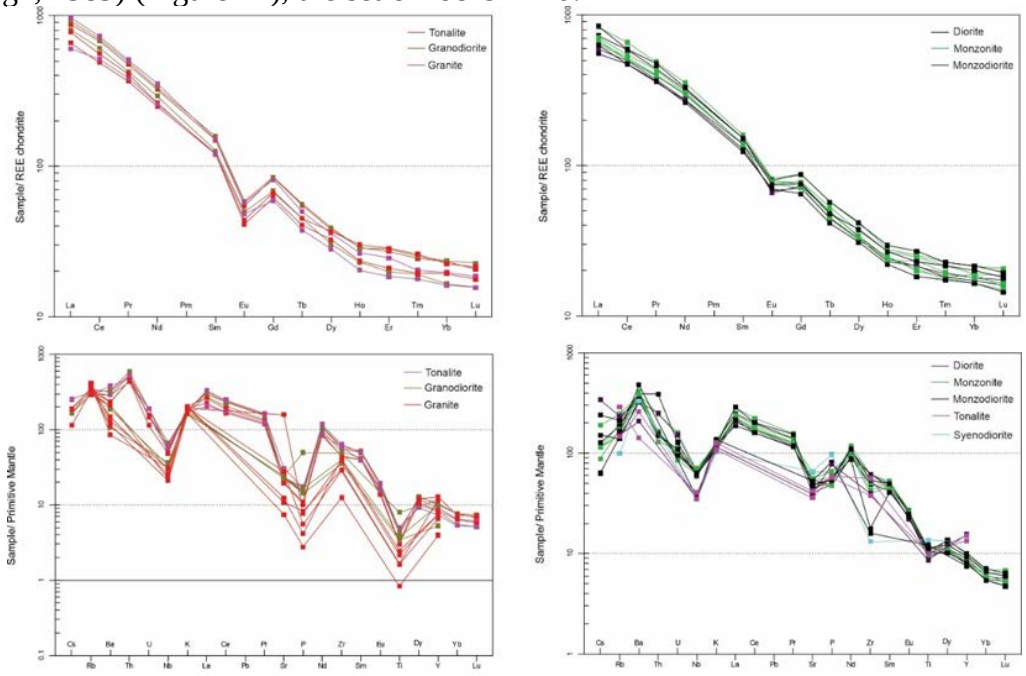

Figure 11 – Multi-elements and Rare Earth Elements (REE) diagrams of the CIC normalized for the chondrite (Boynton, 1984) and the primitive mantle (Sun & McDonough 1989).

The set of rocks from group 1 presents a pattern with negative anomalies in Ti, P, Sr, and Nb, differing only for a strongly positive anomaly in Zr, in addition to Th and Nd.

The granitoids of the CIC can be classified as ferrous to weakly metaluminous, alkali-calcic to calc-alkaline, with a positive trend between the silica content and the Na_2O+K_2O-CaO

parameter, and meta- to peraluminous saturated in silica, according to the diagrams of Frost & Frost (2008) (Figure 12). The classification proposed by Hollocher et al. (2012) determines the rocks of group 2 as having originated in alkaline arc environments. (Figure 13)

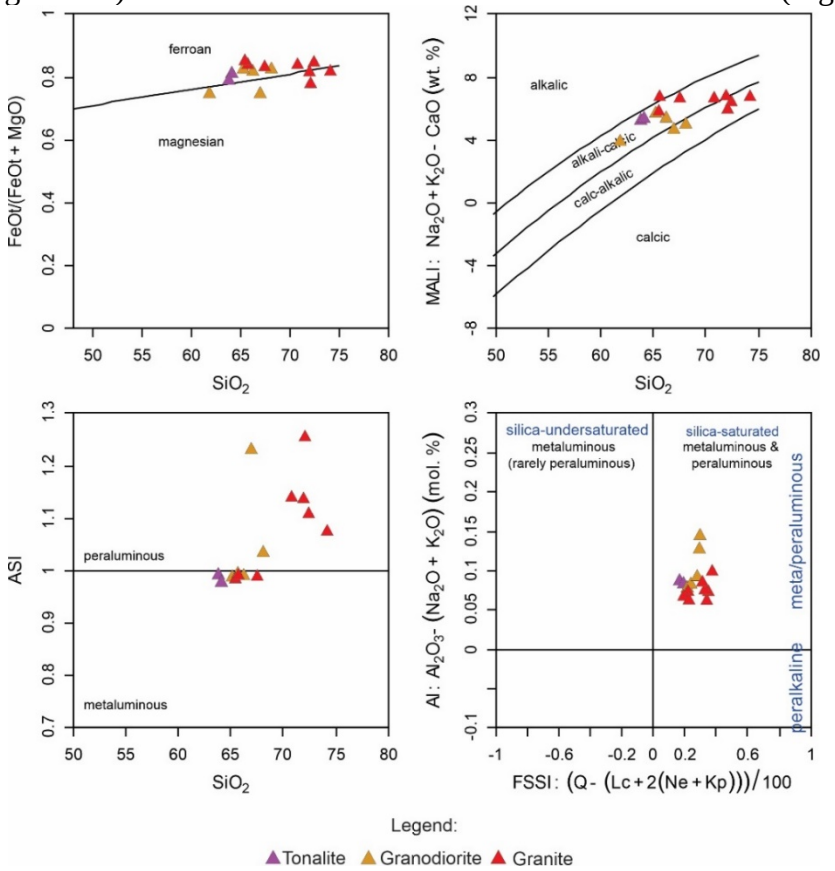

Figure 12 - $FeO^t/(FeO^t + MgO)$ *vs.* SiO_2 diagram according to Frost and Frost (2008). B) SiO_2 *vs.* Na_2O+K_2O-CaO diagram according to Frost and Frost (2008). C) SiO_2 *vs.* ASI diagram according to Frost and Frost (2008). D) FSSI *vs.* AI diagram according to Frost and Frost (2008).

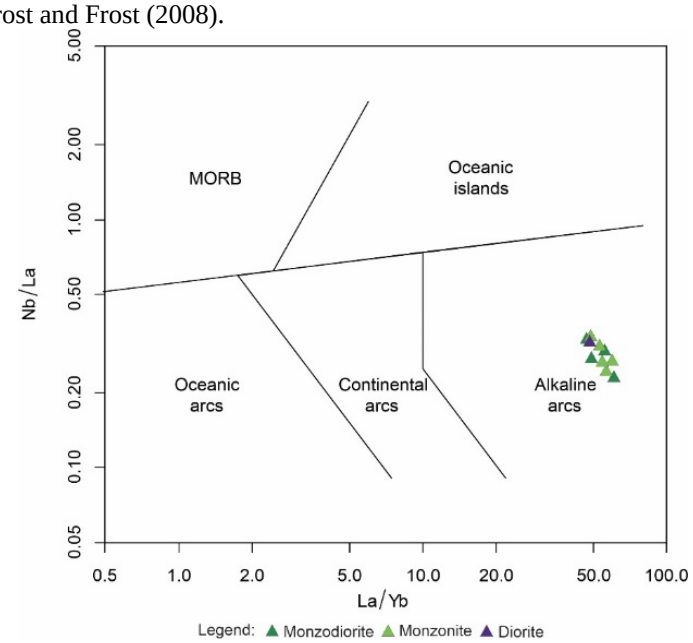

Figure 13 - Tectonic discrimination diagram for the rocks of group 2 of the CIC, according to Hollocher et al. (2012).

U-Pb Geochronology

Three samples from the CIC were analyzed, two of which were related to granites from the northern and western edges of the massif, and the diorite located in the core. Analytical results are presented in supplementary material B. Sample FGIL 01, corresponding to the granite from the northern edge, presents euhedral zircon crystals, prismatic habits, compositional zonation, and homogeneous cores (Figure 14).

From 18 zircon grains analyses, only 5 were used to build a Concordia diagram with an upper intercept age of 504 ± 6 My and MSWD of 0.62 (Figure 15).

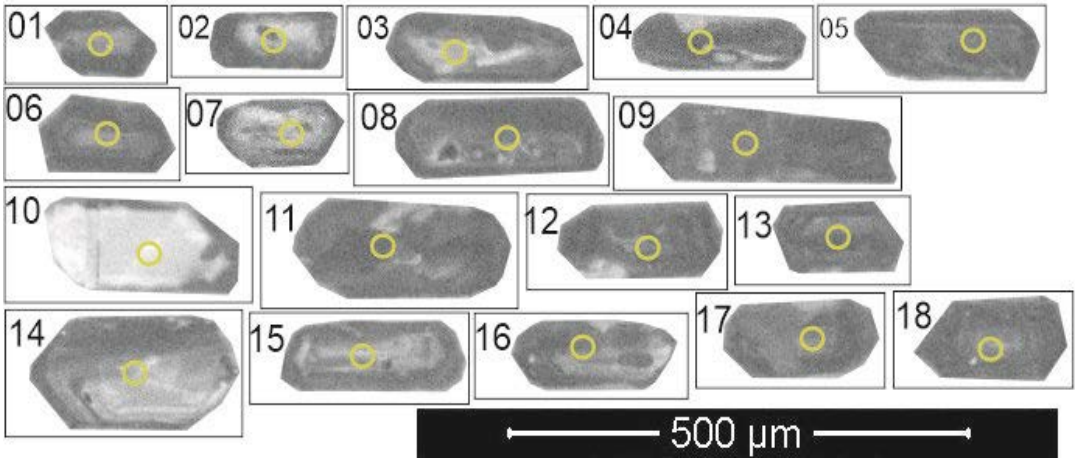

Figure 14 - Cathodoluminescence images of sample FGIL 01. The yellow circles correspond to the U-Pb spots.

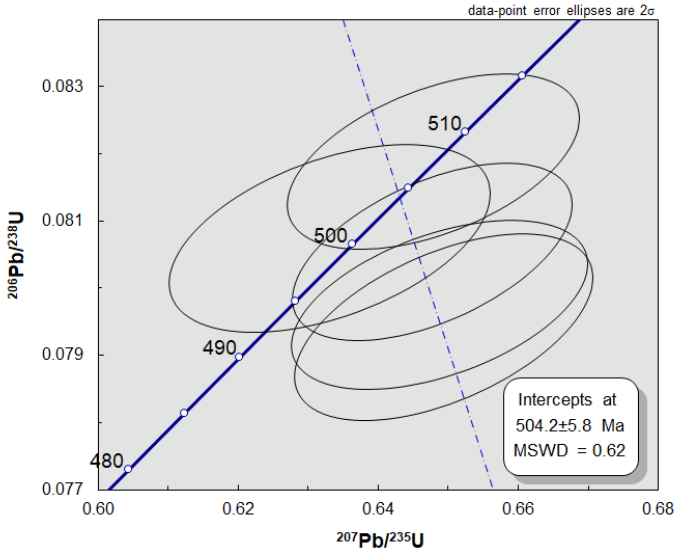

Figure 15 - Concordia diagram for sample FGIL 01 (n=5) results yielded a crystallization age of 504 ± 6 My and MSWD of 0.62.

Sample FGIL 37 corresponds to the diorite from the massif's core. The zircon crystals are euhedral to subhedral and show prismatic to subrounded habits, compositional zonation, and homogeneous colors (Figure 16). From 18 zircon grains analyses, only 8 were used to build the Concordia diagram. This sample yielded a crystallization age of 514 ± 6 My and MSWD of 0.032 (Figure 17).

Sample FGIL 45 corresponds to the granite from the western edge of the CIC. The zircon crystals are euhedral and show prismatic habits, sometimes with bipyramidal terminations, compositional zonation, and homogeneous cores (Figure 18).

From 18 zircon grains analyses, only 8 were used to build the Concordia diagram with an upper intercept age. This sample yielded a crystallization age of 530 ± 4 My and an MSWD of 2.7 (Figure 19).

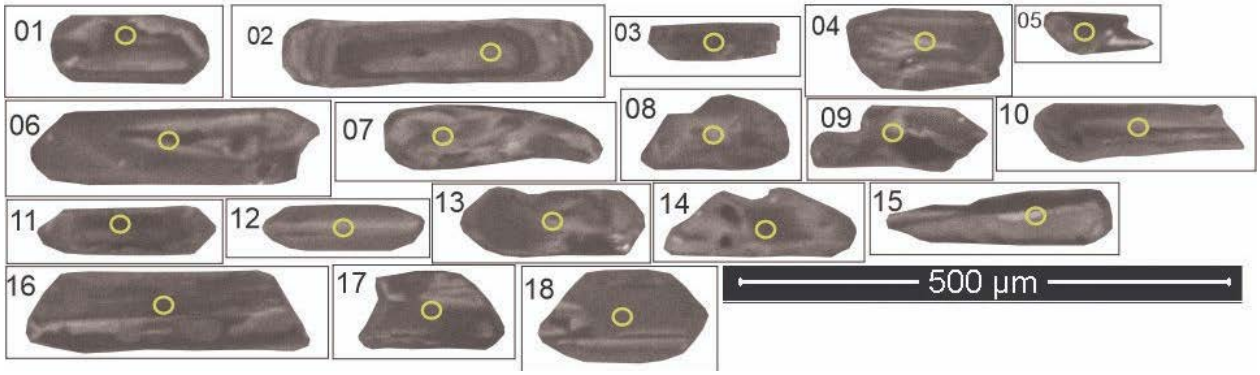

Figure 16 - Cathodoluminescence images of sample FGIL 37. The yellow circles correspond to the U-Pb spots.

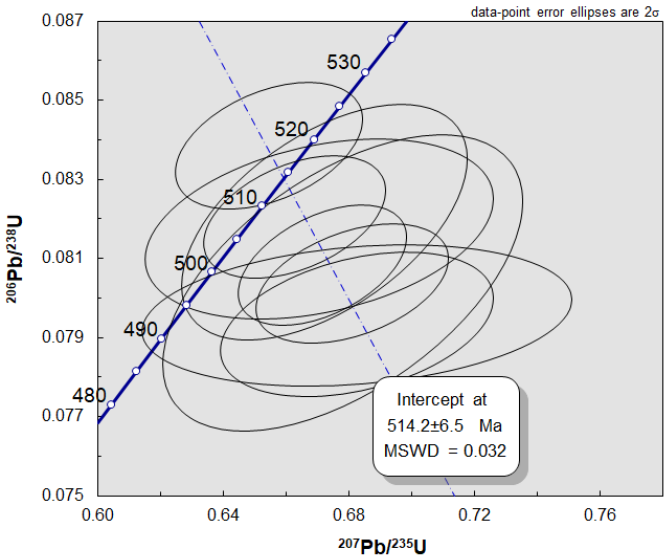

Figure 17 - Concordia diagram for sample FGIL 37 (n=8) yielded a crystallization age of 529 ± 3 My and MSWD of 2.7.

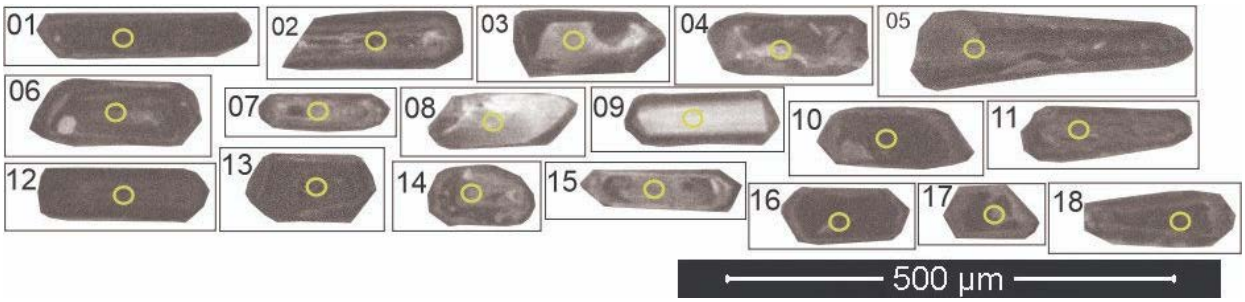

Figure 18 - Cathodoluminescence images of sample FGIL 45. The yellow circles correspond to the U-Pb spots.

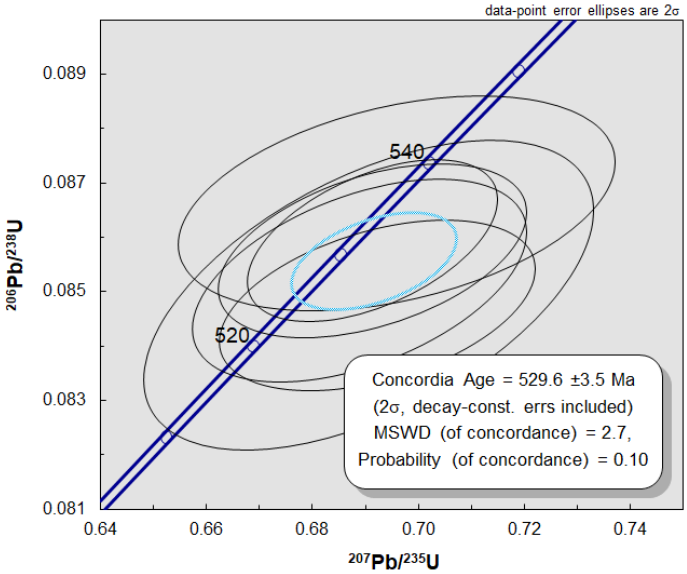

Figure 19 - Concordia diagram for sample FGIL 45 (n=6) yielded a crystallization age of 529 ± 3 My and MSWD of 2.7.

Most of the studied population of zircon grains show magmatic texture growth, as indicated by the CL image. Thus, the domains show zoned during magmatic present U and Th concentrations do not show apparent relationships with grain $^{207}Pb/^{235}U$ age (Figure 20). A progressive increase in Th/U with magmatic fractionation would be consistent with U higher zircon partition coefficient relative to Th. In any case, it is important to note that the higher Th/U ratio in magmatic grains resulting from the magmatic fractionation process is opposite to the commonly observed relationship of decreased Th/U ratio in metamorphic zircons.

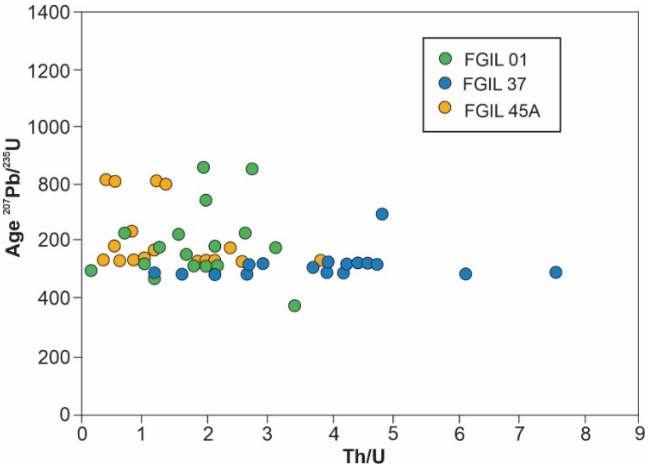

Figure 20 - Age $^{207}Pb/^{235}U$ (Ma) versus Th/U for the zircon grains here studied.

DISCUSSIONS

The mixing process: field and petrographic evidence

CIC shows a diversity of rocks and field features suggesting contrasting magmas (Silva, 1992; Vieira & Menezes, 2015) here interpreted as results of mixing processes. This same process is observed in other intrusive complexes of the G5 super suite as well as in other plutons in Brazil and the world, for example (De Campos et al., 2016; Zhang et al., 2016; Grogan & Reavy, 2002; Alves et al., 2021; Sousa et al., 2022). The main field observed in the CIC that points to a process of magma mixing is the mafic microgranular enclaves, recurrent in the monzogranites, pillow-like dikes, net-veined, and migration of feldspar megacrysts.

The map presented in this work results from extensive facies mapping work in the CIC, which has been developed to standardize the different maps presented so far. The diversity of rocks present in the CIC is evident in all works. Monzogranite and porphyritic monzogranite are the main units in the CIC and is related to the highest altitudes and steep reliefs with K-feldspar phenocrysts that reach six cm and indicate magmatic flow.

Both have the same mineralogy and are cut by pegmatite veins and dikes. Granodiorite and quartz-monzodiorite are predominant units in the south-central portion of the massif (Figure 3). However, quartz-monzodiorite is present in a restricted form in other portions of the CIC.

They are mesocratic to melanocratic rocks, fine-grained, frequently cut by coarse-grained granite injections. The granodiorite presents a salt-and-pepper texture and microgranular mafic enclaves, small plagioclase xenocrysts, mostly rounded, and clots of mafic minerals of a few centimeters. The quartz-monzodiorite is the unit that presents the most features related to magma mixing, such as chilled margins, features analogous to pillows, rounded, corroded feldspar xenocrysts, inclusion zones of mafic minerals in the xenocrysts, mixing zones, compositional zoning, plagioclase laths with evidence of corrosion on the edges, boxy cellular textures, synesis, zones of mafic minerals, crystalline in-version, a mix of apatite crystals and poikilitic texture.

Diorite is the unit that outcrops in the core of the massif in a region of low topography surrounded by granite scarps. It is melanocratic, equigranular, medium to coarse-grained, presents mafic clots of a few centimeters, and is frequently cut by coarse-grained granite injections. Aggregates of biotite and hornblende are common, as are quartz xenocrysts, which show the ocellar quartz-hornblende texture when surrounded by hornblende crystals (Figure 3).

According to Hibbard (1995), a single texture cannot be used as evidence of magma mixing but rather a set of them in the CIC. However, when we consider all the petrographic features such as micro granular mafic enclaves, features analogous to schlieren and agmatic structures, we may suggest the presence of magma mixing.

Microgranular mafic enclaves in the host monzogranite are recurrent in the CIC and may be considered that microgranular mafic enclaves would be the result of the mixing of felsic and mafic magmas. However, the rocks here studied can be interpreted as “bubbles” or “globules” that were produced in the mantle and mixed with felsic rocks of crustal origin.

The enclaves, in this case, may be interpreted as remnants of the partial melting of the rock that gave rise to the granitoids; therefore, the enclaves

would be residues of the most refractory minerals. In the case of the CIC, some textures in the mafic enclaves point to an interaction between two contrasting magmas. The rounded shapes indicate the disintegration of the mafic magma with the felsic magma. The fine grain of the enclaves probably consists of rapid crystallization due to thermal equilibrium between a high-temperature magma and a low-temperature magma.

The cooled margins and syn-plutonic dikes suggest temperature differences between the magmas that mix. K-feldspar phenocrysts occur in enclaves as xenocrysts. This happens when phenocrysts from the host rock can overcome the edges of microgranular mafic enclaves and crystallize within them. The mechanisms for a phenocryst to become a xenocryst involve mechanical migration or capture processes, where partial dissolution of K-feldspar crystals is common, making them rounded.

Crenulated, lobed, and cusp contacts reinforce the existence of different magmas coexisting, which had low viscosity and/or high resistance to flow when they came into contact. Petrographic evidence such as zoned crystals, box cellular and synneusis textures in plagioclase, corroded and rounded crystals, ocellar quartz, mafic mineral clots, acicular apatite and poikilitic crystals are indicative of mixing between mafic and felsic magmas.

Zonation is indicative of sudden variations in crystallization conditions, such as composition and nucleation, and growth rates of crystals, representing an excellent record of thermodynamic variations during magma mixing. The boxy cellular texture in plagioclases can be interpreted as the result of a high growth rate and low nucleation rate. The cooling of the environment caused by heat transfer from the heat to the cooler magma during mixing may be ideal for forming the texture.

Plagioclase with poikilitic texture is also formed by thermal disequilibrium with the matrix of fine-grained mafic rocks. Plagioclase crystals present inclusions of minerals such as quartz, hornblende, biotite, and opaques minerals. Fine graining and plagioclase laths are common in hybrid rocks, which form due to relatively rapid crystallization, favoring a high nucleation rate. The formation of the synneusis texture occurs by the joining of plagioclase crystals suspended in the magma.

Quartz mantled by ocellar hornblende consists of a coarse-grained and rounded quartz xenocryst with inclusions of tiny hornblende crystals on its rim.

Both major and trace elements principal component analysis reinforce the formation of two groups of rocks at different times and sources. The correlation matrices between the principal components reveal the prominent role of the magma mixing process. The low values observed in general (colors in shades of blue) show a strong correlation between the elements and the effectiveness of the mixing process. The strong correlation between the elements is facilitated in the mixing process by the diffusion process of the chemical elements present in the different magmas.

U-Pb interpretations

The new U-Pb data in zircon here reported confirm that the peak of magma pro-duction in the CIC (Figure 21) corresponds to the post-collisional stage of the Araçuaí Orogeny, between 530 and 480 My (De Campos et al., 2004; Serrano et al., 2018; Aranda et al., 2020; Araujo et al., 2020; Duffles Teixeira et al., 2020; Melo et al., 2020; Potratz et al. 2022; Bellon et al., 2022).

The U-Pb analyses for the rocks of the CIC presented here are correlated with the data reported in the literature. Isotopic studies of $^{87}Sr/^{86}Sr$ and $^{143}Nd/^{144}Nd$ presented by De Campos et al. (2004) and references therein suggested that the gabbroic rocks of the G5 supersuite are the product of partial melting of a previously enriched mantle during the onset of subduction in the Araçuaí Orogeny.

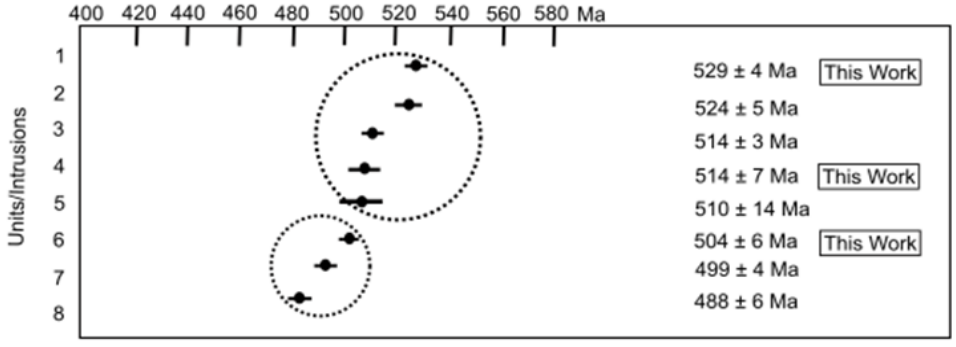

Figure 21 - U-Pb ages in zircon grains of the CIC reported in the literature and this work.

A previously enriched mantle may be one of the sources for the generation of basaltic magmas, which is partially corroborated by the low $^{176}Hf/^{177}Hf$ ratios obtained by (Macedo et al., 2022) for the quartz-monzodiorite of the CIC. However, Macedo et al. (2022) also obtained zircon grains with high $^{176}Hf/^{177}Hf$ ratios and positive $\varepsilon_{Hf(t)}$ values for this same quartz-monzodiorite from the CIC, which demonstrates that a depleted mantle component is also present. Here, an important discussion arises regarding the mantle source of the G5 supersuite: does only one mantle reservoir act as a source, or, as with magmatism associated with mantle plumes, is more than one mantle reservoir present?

In addition, the Lu-Hf data reported by Macedo et al. (2022) are used here to constrain the sources of the study rocks. Three samples of monzogranite, one sample of quartz-diorite, and one sample of hololeucocratic dike.

According to Macedo et al. (2022) the U-Pb zircon ages for the CIC show a peak of magma production around 500 ± 15 My, ranging from 527 ± 3 My to 427 ± 5 My. Three analyses were performed on zircon grains from the monzogranitic component, one on a quartz-diorite sample and one on a hololeucocratic dike sample. As reported by Macedo et al. (2022), the samples analyzed show positive and negative values of $\varepsilon_{Hf(t)}$, with maximum values between +12.70 and -39.5. The model ages (T_{DM}) presented range from the Paleoproterozoic to the Neoproterozoic, showing a pattern of Paleoproterozoic ages for negative $\varepsilon_{Hf(t)}$ values. In contrast, the Neoproterozoic ages are related to positive $\varepsilon_{Hf(t)}$ values.

Table 2 - Summary of U-Pb geochronological and Lu-Hf isotopic data from the CIC, compiled from Macedo et al. (2022).

Sample	Rock	U-Pb age (My)	MSWD	$^{176}Hf/^{177}Hf$	$\varepsilon_{Hf(t)}$	T_{DM} ages (Gy)
FGIL 06 A	Monzogranite	499 ± 4	1.12	0.28142 to 0.28268	+10.7 and -13.2	0.75 to 2.11
FGIL 11 A	Monzogranite	524 ± 5	1.4	0.28134 to 0.28275	+12.6 and- 22.0	0.64 to 2.60
FGIL 17 A	Monzogranite	521 ± 14	0.49	0.28142 to 0.28300	+11.3 and -24.0	0.72 to 2.71
FGIL 06 B	Qtz Monzodiorite	486 ± 12	0.43	0.28181 to 0.28281	+12.5 and-22.7	0.65 to 2.64
FGIL 06 C	Hololeucocratic dyke	432 ± 32	1.17	0.28155 to 0.28281	+12.7 and -24.0	0.64 to 2.71

The significant variation between the $\varepsilon_{Hf(t)}$ values, which reach around 30 units, can be explained by the interaction process of magma originating from the crust and the mantle. This variation is observed within each sample analyzed, corroborating that the zircons in these rocks have distinct isotopic compositions and were subsequently agglutinated in the same volume of rock, preserving this considerable isotopic variation. Some plutons of the Araçuaí Orogeny also exhibit positive and negative values of $\varepsilon_{Hf(t)}$, as is the case of the Afonso Cláudio, Barra de São Francisco and Santa Angélica Intrusive Complexes (Aranda et al., 2020; Melo et al., 2020; Potratz et al., 2020) corroborating the fact that different sources of magmas were present in the formation of these massifs, and which are also confirmed by field, petrographic and lithogeochemical evidence, unlike that suggested for the Várzea Alegre and Venda Nova Intrusive Complexes (Onken et al., 2024), which do not take into account the evidence of magma mixing, including that suggested by other authors for the same massifs (De Campos et al., 2004; Aranda et al., 2020; Melo et al., 2020; Bellon et al., 2022).

The T_{DM} ages range from 2.7 Ga to 1.41, and together with the $\varepsilon_{Hf(t)}$ values, they corroborate with different magma sources for the CIC, one mantle source, and at least two crustal sources. The negative $\varepsilon_{Hf(t)}$ values observed in all samples show Neoproterozoic T_{DM} ages, ranging from 0.64 My to 1.18 My, thus constituting an important juvenile reservoir. The $\varepsilon_{Hf(t)}$ values between -26 and -22 present Archean T_{DM} ages (2.6 to 2.4 Gy), while the samples with $\varepsilon_{Hf(t)}$ values between -17 to -8 are essentially Paleoproterozoic (2.2 Gy to 1.7 Gy).

Araujo et al. (2020) and Potratz et al. (2022) discuss the possibility of different crustal sources for the Pedra Azul and Santa Angélica Intrusive Complexes, respectively. As observed in the CIC, an older crustal source appears in both. Therefore, some candidates appear as possible older crustal sources. Faria et al. (2022) report Archean and Paleoproterozoic T_{DM} ages, in addition to positive and negative values of $\varepsilon_{Hf(t)}$ for rocks of the Caparaó Complex, showing similarities with the signatures observed in the CIC. Other possible candidates that are presented are the Juiz de Fora and Pocrane Complexes, basements of the Araçuaí Orogeny (Noce et al.,

2007; Degler et al., 2018; Lana et al., 2020). The rocks of the Juiz de Fora and Pocrane Complex, which represent the basement of the Araçuaí Orogeny, also present positive and negative values for $\varepsilon_{Hf(t)}$ and $\varepsilon_{Nd(t)}$, in addition to TDM ages in the Archean to Paleoproterozoic transition.

An important Neoproterozoic candidate for the crustal source of the CIC is the granitoids of the G1 supersuite (Pedrosa-Soares et al., 2001). Hf and Nd data for rocks of the Estrela Orthogneiss in the Castelo region indicate values ranging from -9.2 to -4.7 and Paleo- to Mesoproterozoic T_{DM} ages ranging from 2.2 to 1.4 Gy (Pereira et al., 2023). The host of the CIC, the Caxixe Batholith (Santiago et al., 2020), presents U-Pb ages in zircon around 850 Ma, correlated with the Serra da Prata magmatic arc of the Ribeira Orogeny (Peixoto et al., 2017). These rocks present positive $\varepsilon_{Hf(t)}$ values, between +10 and +14, and a Neoproterozoic model age. Santiago et al. (2023) also present for the Caxixe Batholith, rocks compatible with the G1 supersuite of the Araçuaí Orogeny, between 630 and 580 My, with negative Hf values, between -4 and -13, and T_{DM} ages between 1.33 and 1.67. This data from the literature and the results reported here are slow to suggest an important crustal contribution for the formation of CIC.

CONCLUSIONS

The conclusions consider field information, geochemistry, U-Pb ages and Lu-Hf and Sm-Nd isotopes (from the literature). All information put together allowed us to suggest multiple sources (mantelic and crustal), and petrographic mixture textures is an indication of magma mixing.

The (CIC) origin reveals a complex interaction between magmas of different compositions and sources, evidenced by both petrographic and structural features and lithogeochemical and isotopic data. Mixing magmas is widely supported by microgranular mafic enclaves, specific textures such as ocellar quartz and K-feldspar phenocrysts, and field features such as syn-plutonic dikes.

In addition to the mixing of magmas, the isotopic data suggests the participation of multiple mantle and crustal sources in the genesis of the CIC, with significant variations in the values of $\varepsilon_{Hf(t)}$ and T_{DM} model ages. These data corroborate the hypothesis of contribution from enriched and depleted mantle reservoirs and multiple crustal sources.

These data indicate a complex interaction of post-collisional magmatic processes in the context of the Araçuaí Orogeny, reinforcing the importance of investigating multiple reservoirs to understand the tectonic-magmatic evolution of this Orogeny.

This mechanism may have been facilitated by the delamination of the very thick litho-sphere with significant elevations with high gravitational potential and the enrichment of the mantle through the slab at the end of the collisional stage. These elements lead to lateral flow that facilitated the intrusion of basic magmas formed by the partial melting of an asthenospheric mantle and crustal magmas generated by the heat provided by the rising mantle.

In this sense, the process of decompression of the lower crust provided sufficient heat for crustal anatexis, where later magmatic mechanisms of physical dispersion (mingling) and chemical diffusion (mixing) favored hybridization.

However, it is considered that this was not a process that occurred all at once; the subtle differences in the chemical and isotopic signatures shown in the rocks of the CIC lead to the belief that several pulses and different portions of the crust were responsible for the formation of the magmas that originated the complex.

Author Contributions:
Conceptualization: Iago Mateus Lopes de Macêdo, Guilherme Loriato Potratz, Marilane Gonzaga de Melo, Mauro Cesar Geraldes, Rodson Marques de Abreu; Methodology: Iago Mateus Lopes de Macêdo, Guilherme Loriato Potratz, Marilane Gonzaga de Melo, Mauro Cesar Geraldes, Rodson Marques de Abreu; formal analysis: Iago Mateus Lopes de Macêdo, Guilherme Loriato Potratz, Mauro Cesar Geraldes, Renzo Dias Rodrigues, Ana Paula Meyer, Armando Dias Tavares, Marco Machado da Silva; investigation: Iago Mateus Lopes de Macêdo, Marilane Gonzaga de Melo, Mauro Cesar Geraldes, Rodson Marques de Abreu; resources: Mauro Cesar Geraldes, Armando Dias Tavares; writing—review and editing: Iago Mateus Lopes de Macedo, Guilherme Loriato Potratz, Mauro Cesar Geraldes; visualization: Iago Mateus Lopes de Macedo, Guilherme Loriato Potratz, Mauro Cesar Geraldes. All authors have read and agreed to the published version of the manuscript.

ACKNOWLEDGMENTS

Iago Mateus Lopes de Macêdo and Guilherme Loriato Potratz thank to Fundação Carlos Chagas Filho de Amparo à Pesquisa do Estado do Rio de Janeiro for doctoral and postdoctoral scholarship, process numbers E26-204.530/2021 and E26-204.531/2021 (respectively) and to CAPES for granted support. Mauro Cesar Geraldes thanks the National Council for Scientific and Technological Development (CNPq) for the research grant (process nº 301470/2016-2).

REFERENCES

ALKMIM, F.F.; MARSHAK, S.; PEDROSA-SOARES, A.C.; PERES, G.G.; CRUZ, S.; WHITTINGTON, A. Kinematic evolution of the Araçuaí-West Congo orogen in Brazil and Africa: Nutcracker tectonics during the Neoproterozoic assembly of Gondwana. **Precambrian Research**, v. 149, p. 43-64, 2006.

ALKMIM, F.F.; KUCHENBECKER, M.; REIS, H.L.S.; PEDROSA-SOARES, A.C. The Araçuaí belt. In: HEILBRON, M., CORDANI, U.G, ALKMIM F.F. (Eds.), **São Francisco Craton, Eastern Brazil**. Regional Geology Reviews, Springer International Publishing Co., p. 255–276, 2017.

ALMEIDA, F.F.M.; BRITO NEVES, B.B.; CARNEIRO, C.D.R. The origin and evolution of the South American Platform. **Earth Sciences Reviews**, v. 50, p. 77-111, 2000.

ALVES, M.I.; ALMEIDA, B.S.; CARDOSO, L.M.C.; SANTOS, A.C.; APPI, C.; BERTOTTI, A.L.; CHEMALE, F.; TAVARES JR, A.D.; MARTONS, M.V.A.; GERALDES, M.C. Isotopic Composition of Lu, Hf, and Yb in GJ-1, 91500 and Mud Tank reference materials measured by LA-ICP-MS: Application of the Lu-Hf geochronology in zircon. **Journal of Sedimentary Environments**, v. 4, n. 2, p. 220-248, 2019

ALVES, A.; JANASI, V.A.; PEREIRA, G.S.; PRADO, F.A.; MUNOZ, P.R.M. Unravelling the hidden evidence of magma mixing processes via combination of in situ Sr isotopes and trace elements analyses on plagioclase crystals. **Lithos**, v. 404-405, p. 106435, 2021.

ARANDA, R.O.; CHAVES, A.O.; MEDEIROS JÚNIOR, E.B.; VENTURINI JUNIOR, R. Petrology of the Afonso Cláudio intrusive complex: new insights for the Cambro Ordovician post-collisional magmatism in the Araçuaí-west Congo Orogeny, southeast Brazil. **Journal of South American Earth Sciences**, v. 98, p. 102465, 2020.

ARAUJO, C.; PEDROSA-SOARESA, A.; LANA, C.; DUSSIN, I.; QUEIROGA, G.; SERRANO, P.; MEDEIROS- JUNIOR, E. Zircon in emplacement borders of post-collisional plutons compared to country rocks: A study on morphology, internal texture, U Th–Pb geochronology and Hf isotopes (Araçuaí Orogeny. SE Brazil). **Lithos**, v. 352–353, p. 105252, 2020.

BALTAZAR, O.F.; ZUCCHETTI, M.; OLIVEIRA, S.A.M.; SCANDOLARA, J.; SILVA, L.C. **Geologia das folhas São Gabriel da Palha e Linhares**. Programa Geologia do Brasil. CPRM–Serviço Geológico do Brasil, Belo Horizonte, 2010.

BAYER, P.; SCHIMIDT-THOMÉ, R.; WEBER-DIEFENBACH, K.; HORN, H.A. Complex concentric granitoid intrusions in the coastal mobile belt, Espírito Santo, Brazil: The Santa Angélica Pluton—An example. **Geologische Rundsch**., v. 76, p. 357–371, 1987,

BELLON, U.D.; SOUZA-JUNIOR, G.F.; TEMPORIM, F.A.; D'AGRELLA-FILHO, M.S.; TRINDADE, R.I.F. U-Pb geochronology of a reversely zoned pluton: Records of pre-to-post colisional magmatism of the Araçuaí belt (SE-Brazil)? **Journal of South American Earth Sciences**, v. 119, p. 104045, 2022.

BONIN, B. Do coeval mafic and felsic magmas in post-collisional to within-plate regimes necessarily. Imply two contrasting, mantle and crustal, sources? A review. **Lithos**, v. 78, p. 1 – 24, 2004

BOYNTON, W.V. Cosmochemistry of the rare earth elements, meteorite studies. In: Henderson, P. (Ed.), **Rare Earth Element Geochemistry**, Elsevier, Amsterdam, v. l., p. 63–114, 1984.

CORRALES F.F.P.; DUSSIN I.A.; HEILBRON M.; BRUNO H.; BERSAN S.A.; VALERIANO C.M.; PEDROSA-SOARES A.C.; TEDESCHI M. Coeval high Ba-Sr arc-related and OIB Neoproterozoic rocks linking pre-collisional magmatism of the Ribeira and Araçuaí Orogenic belts, SE-Brazil. **Precambrian Research**, v. 337, p. 105476, 2020.

DE CAMPOS, C.P. Chaotic flow patterns from a deep plutonic environment: A case study on natural magma mixing. **Pure Applied Geophysics**, v. 172, p. 1815–1833, 2015.

DE CAMPOS, C.P.; MENDES, J.C.; LUDKA, I.P.; MEDEIROS, S.R.; MOURA, J.C.; WALLFASS, C. A review of the Brazilian magmatism in southern Espirito Santo, Brazil, with emphasis on post collisional magmatism. **Journal Virtual Explorer**, v. 17, p. 1–35, 2004.

DE CAMPOS, C.P.; MEDEIROS, S.R.; MENDES, J.C.; PEDROSA-SOARES, A.C.; DUSSIN, I.; LUDKA, I.P.; DANTAS, E.L. Cambro-Ordovician magmatism in the Araçuaí Belt (SE Brazil): Snapshots from a post-collisional event. **Journal of South American Earth Sciences**, v. 68, p. 248–268, 2016.

DE LA ROCHE, H.; LETERRIER, J.; GRANDE CLAUDE, P.; MARCHAL, M. A volcanic and plutonic rocks classification using R1–R2 diagrams and major element analyses – Its relationships and current nomenclature. **Chemical Geology**, v, 29, p. 183–221, 1980.

DEGLER, R.; PEDROSA-SOARES, A.; NOVO, T.; TEDESCHI, M.; SILVA, L.C.; DUSSIN, I.; LANA, C. Rhyacian-Orosirian isotopic records from the basement of the Araçuaí-Ribeira orogenic system (SE Brazil): links in the Congo-São Francisco paleocontinent. **Precambrian Research**, v. 317, p. 179–195, 2018.

DUFFLES TEIXEIRA, P.A.; FERNANDES, C.M.; MENDES, J.C.; MEDEIROS, S.R.; ROCHA, I.S.A. U-Pb LA-ICP-MS and geochemical data of the Alto Chapéu Pluton: contributions on bimodal post-collisional magmatism in the Araçuaí belt (SE Brazil). **Journal of South American Earth Sciences**, v. 103, 102724, 2020.

FARIA, T.G.; ALVES, M.I.; POTRATZ, G.L.; DA SILVA, L.F.R.; RODRIGUES, S.W.; MARTINS, M.V.A.; GERALDES, M.C. The Serra do Caparaó Complex, Mantiqueira Province, Brazil, revisited: metamorphic age constraints by U-Pb and Lu-Hf method in zircon by LA-ICP-MS. **Journal of the Geological Survey of Brazil**, v. 5, n. 1, p.49-80, 2022.

FROST, B.R. & FROST, C.D. A Geochemical classification for feldspathic igneous rocks. **Journal of Petrology.**, v. 49, p. 1955–1969, 2008.

GAGNEVIN, D.; DALY, J.S.; KRONZ, A. Zircon texture and chemical composition as a guide to magmatic processes and mixing in a granitic environment and coeval volcanic system. **Contributions Mineral Petrology**, v. 159, p. 579–596, 2010.

GONÇALVES, L.; FARINA, F.; LANA, C.; PEDROSA-SOARES, A.C.; ALKMIM, F.; NALINI JR.; H.A. New U-Pb ages and lithochemical attributes of the Ediacaran Rio Doce magmatic arc, Araçuaí confined Orogeny, southeastern Brazil. **Journal of South American Earth Sciences**, v. 52, p. 129–148, 2014.

GONÇALVES, L.; ALKMIM, F.F.; PEDROSA-SOARES, A.C.; DUSSIN, I.A.; VALERIANO, C.M.; LANA, C.; TEDESCHI, M. Granites of the intracontinental termination of a magmatic arc: an example from the Ediacaran Araçuaí Orogeny, southeastern Brazil. **Gondwana Research**, v. 36, p. 439–458, 2016.

GONÇALVES, L.; ALKMIM, F.F.; PEDROSA-SOARES, A.C.; GONÇALVES, C.C.; VIEIRA, V.; From the plutonic root to the volcanic roof of a continental magmatic arc: a review of the

Neoproterozoic Araçuaí Orogeny, southeastern Brazil. **International Journal Earth Sciences**, v. 107, p. 337–358, 2018.

GRADIM, C.; RONCATO, J.; PEDROSA-SOARES, A.C.; CORDANI, U.; DUSSIN, I.; ALKMIM, F.F.; QUEIROGA, G.; JACOBSOHN, T.; SILVA, L.C.; BABINSKI, M. The hot back-arc zone of the Araçuaí Orogeny, Eastern Brazil: From sedimentation to granite generation. **Brazilian Journal of Geology**, v. 44, p. 155–180, 2014.

GROGAN, S.E. & REAVY, R.J. Disequilibrium textures in the Leinster Granite Complex, SE Ireland: evidence for acid-acid magma mixing. **Mineralogical Magazine**, v. 66, n. 6, p. 929–939, 2002.

HEILBRON, M.L.; PEDROSA-SOARES, A.C.; CAMPOS NETO, M.C.; SILVA, L.C.; TROUW, R.; JANASI, V.A. Brasiliano Orogeny's in Southeast and South Brazil. **Journal Virtual Explorer 17**, Paper 4, 2004.

HIBBARD, M.J. **Petrography to Petrogenesis**. Prentice Hall, Englewood Cliffs, New Jersey, 587p., 1995.

HOLLOCHER, K.; ROBINSON, P.; WALSH, E.; ROBERTS, D. Geochemistry of amphibolite-facies volcanic and gabbros of the Storen nappe in extensions west and southwest of Trondheim, Western Gneiss Region, Norway: A key to correlations and paleotectonic settings. **American Journal of Sciences**, v. 312, p. 357–416, 2012.

JACKSON, S.E.; PEARSON, N.J.; GRIFFIN, W.L.; BELOUSOVA, E.A. Applying laser ablation-inductively coupled plasma-mass spectrometry to in situ U-Pb zircon geochronology. **Chemical Geology,** v. 211, n. 1–2, p. 47–69, 2004.

LANA, C.; MAZOZ, A.; NARDUZZI, F.; CUTTS, K.; FONSECA, M. Paleoproterozoic sources for Cordilleran-type Neoproterozoic granitoids from the Araçuaí Orogeny (SE Brazil): constraints from Hf isotope zircon composition. **Lithos**, v. 378, 105815, 2020.

LIÉGEOIS, J.P. Some words on the post-collisional magmatism – Preface to Special Edition on Post-collisional Magmatism. **Lithos**, v. 45, p. xv-xvii, 1998.

MACEDO, I.M.L.; GERALDES, M.C.G.; MARQUES, R.A.; MELO, M.G.; TAVARES, A.D.; MARTINS, M.V.A.; OLIVEIRA, H.C.; RODRIGUES, R.D. New clues for magma-mixing processes using petrological and geochronological evidence from the Castelo Intrusive Complex, Araçuaí Orogeny (SE Brazil). **Journal of South American Earth Sciences**, v. 115, p. 103758, 2022.

MARTINS, V.T.S.; TEIXEIRA, W.; NOCE, C.M.; PEDROSA-SOARES, A.C. Sr and Nd characteristics of Brasiliano/ Panafrican granitoid plutons of the Araçuaí Orogeny, southeastern Brazil: tectonic implications. **Gondwana Research**, v 7, p. 75–89, 2004.

MEDEIROS, J.D.C. **Caracterização petrográfica e litogeoquímica do Batólito Forno Grande, Castelo, Espírito Santo**. Alegre, 2013, p. 96. Graduation Work Final – Universidade Federal do Espírito Santo.

MEDEIROS, S.R.; WIEDEMANN, C.M.; VRIEND, S. Evidence of mingling between contrasting magmas in a deep plutonic environment: the example of Várzea Alegre in the Panafrican/Brasiliano Mobile Belt in Brazil. **Anais da Academia Brasileira de Ciências**, v. 73, p. 99–119, 2001.

MELO, M.G.; LANA, C.; STEVENS, G.; HARTWIG, M.E.; PIMENTA, M.S. Deciphering the source of multiple U-Pb ages and complex Hf isotope composition in zircon from post-collisional charnockite-granite associations from the Araçuaí Orogeny (southeastern Brazil). **Journal of South American Earth Sciences**, v. 103, p. 102792, 2020.

MELO, M.G.; STEVENS, G.; LANA, C.; PEDROSA-SOARES, A.C.; FREI, D.; ALKMIM, F.F.; ALKMIM, L. A. Two cryptic anatectic events within a syn-collisional granitoid from the Araçuaí Orogeny (southeastern Brazil): evidence from the polymetamorphic Carlos Chagas batholith. **Lithos,** v. 277, p. 51–71, 2017a.

MELO, M.G.; LANA, C.; STEVENS, G.; PEDROSA-SOARES, A.C.; GERDES, A.; ALKMIM, L.A.; NALINI JR., H.A.; ALKMIM, F.F. Assessing the isotopic evolution of S-type granites of the Carlos Chagas Batholith, SE Brazil: clues from U–Pb, Hf isotopes, Ti geothermometry and trace element composition of zircon. **Lithos**, v. 284–285, p. 730–750, 2017b.

MENDES, J.C. & DE CAMPOS, C.M.P. Norite and charnockites from the Venda Nova Pluton, SE Brazil: intensive parameters and some petrogenetic constraints. **Geosciences Frontiers**, v. 3, p. 789–800, 2012.

MENDES, J.C.; MEDEIROS, S.R.; MCREATH, I.; DE CAMPOS, C.M.P. Cambro-ordovician magmatism in SE Brazil: U-Pb and Rb-Sr ages, combined with Sr and Nd isotopic data of charnockitic rocks from the Várzea Alegre complex. **Gondwana Research**, v. 8, p. 337–345, 2005.

MEYER, A.P. **Geologia e geoquímica da porção sul do Maciço Castelo-ES**. Rio Claro, 143 p. 2017. PhD Thesis. Universidade Estadual Paulista, Instituto de Geociências e Ciências Exatas.

NOCE, C.M.; PEDROSA-SOARES, A.C.; SILVA, L.C.; ARMSTRONG, R.; PIUZANA, D. Evolution of polycyclic basement complexes in the Araçuaí Orogen, based on U-Pb SHRIMP data: implication for Brazil-Africa links in Paleoproterozoic time. **Precambrian Research,** v. 159, p. 60–78, 2007.

ONKEN, C.T.; EBERHARD-SCHMID, J.; HAUSER, L.; MARIONI, S.; GALLI, A.; JANASI, V. A.; SCHMIDT, M.W. Timing and origin of the post-collisional Venda Nova and Várzea Alegre Plutons from the Araçuaí belt, Espírito Santo, Brazil. **Lithos**, v. 482, p. 107677, 2024.

PEDROSA-SOARES, A.C.; NOCE, C.M.; WIEDEMANN, C.M.; PINTO, C.P. The Araçuaí-West Congo Orogeny in Brazil: An overview of a confined Orogeny formed during Gondwanland assembly. **Precambrian Research**, v. 110, p. 307–323, 2001

PEDROSA-SOARES, A.C.; CAMPOS, C.P.C., NOCE, C., SILVA, L.C.; NOVO, T.; RONCATO, J.; MEDEIROS, S.; CASTANEDA, C.; QUEIROGA, G.; DANTAS, E.; DUSSIN, I.; ALKMIM, F. Late Neoproterozoic-Cambrian granitic magmatism in the Araçuaí Orogeny (Brazil), the Eastern Brazilian Pegmatite Province and related mineral resources. In: SIAL, A.N., BETTENCOURT, J.S., DE CAMPOS, C.P., FERREIRA, V.P. (Eds.), **Granite-Related Ore Deposits**. Geological Society, Special Publications, London, p. 25–51, 2011.

PEDROSA-SOARES, A.C.; DELUCA, C.; ARAUJO, C.; GRADIM, C.; LANA, C.; DUSSIN, I.; SILVA, L.C.; BABINSKI, M. O Orógeno Araçuaí à luz da geocronologia: um tributo a Umberto Cordani. In: BARTORELLI, A.; TEIXEIRA, W.; BRITO NEVES, B.B. (Eds.), **Geocronologia e Evolução Tectônica do Continente Sul-Americano: a contribuição de Umberto Giuseppe Cordani**. Solarias Edições Culturais, São Paulo, 2020, p. 728p.

PEIXOTO, E.; PEDROSA-SOARES, A.C.; ALKMIM, F.F.; DUSSIN, I.A. A suture-related accretionary wedge formed in the Neoproterozoic Araçuaí Orogeny (SE Brazil) during Western Gondwanaland assembly. **Gondwana Research**, v. 27, p. 878–896, 2015.

PEIXOTO, C.A.; HEILBRON, M.; RAGATKY, D.; ARMSTRONG, R.; DANTAS, E.; VALERIANO, C.M.; SIMONETTI, A. Tectonic evolution of the Juvenile Tonian Serra da Prata magmatic arc in the Ribeira belt, SE Brazil: implications for early West Gondwana amalgamation. **Precambrian Research**, v. 302, p. 221–254, 2017.

PEREIRA, V.H.; MENDES, J.; CARVALHO, M.; COELHO, V.; MEDEIROS, S.; VALERIANO, C. Petrogenesis of Estrela is granitoid and implications for the evolution of the Rio Doce magmatic arc: Araçuaí-Ribeira Orogenic system, SE Brazil. **Journal of South American Earth Sciences**, v. 126, p. 104337, 2023.

PERUGINI, D.; PETRELLI, M.; POLI, G.; DE CAMPOS, C.; DINGWELL, D.B. Recent phlegrean field eruptions' timescales are inferred from applying a "diffusive fractionation" model of trace elements. **Bulletin of Volcanology**, v. 72, p. 431–447, 2010.

PERUGINI, D.; DE CAMPOS, C.P.; DINGWELL, D.B.;

DORFMAN, A. Relaxation of concentration variance: a new tool to measure chemical element mobility during mixing of magmas. **Chemical Geology**, n. 335, p. 8–23, 2013.

PETITGIRARD, S.; VAUCHEZ, A.; EGYDIO-SILVA, M.; BRUGUIER, O.; CAMPS, P.; MONI´E, P.; BABINSKY, M.; MONDOU, M. Conflicting structural and geochronological data from the Ibiturana quartz-syenite (SE Brazil): effect of protracted "hot" Orogeny and slow cooling rate? **Tectonophysics**, v. 477, p. 174–196, 2009.

POTRATZ, G.L.; GERALDES, M.C.; MEDEIROS-JUNIOR, E.B.; TEMPORIM, F.A.; MARTINS, M.V.A. A Juvenile Component in the Pre- and Post-Collisional Magmatism in the Transition Zone between the Araçuaí and Ribeira Orogenic (SE Brazil). **Minerals**, v. 12, p. 1378, 2022.

RICHTER, F.; LANA, C.; STEVEN, G.; BUICK, I.; PEDROSA-SOARES, A.C.; ALKMIM, F.F.; CUTTS, K. Sedimentation, metamorphism and granite generation in a back-arc region: Records from the Ediacaran Nova Venecia Complex (Araçuaí Orogeny, South-eastern Brazil). **Precambrian Research**, v. 272, p. 78–100, 2016.

SAMI, M.; NTAFLOS, T.; FARAHAT, E.S.; MOHAMED, H.A.; HAUZENBERGER, C.; AHMED, A.F. Petrogenesis and geodynamic implications of Ediacaran highly fractionated A type granitoids in the north Arabian-Nubian Shield (Egypt): constraints from whole rock geochemistry and Sr-Nd isotopes. **Lithos**, v. 304(307), p. 329–346, 2018.

SANTIAGO, R.; CAXITO, F.A.; PEDROSA-SOARES, A.C.; NEVES, M.; DANTAS, E.L. Toniana Island Arc Remnants in the Northern Ribeira Orogeny of Western Gondwana: the Caxixe Batholith (Espírito Santo, SE Brazil). **Precambrian Research**, p. 105944, 2020.

SANTIAGO, R., CAXITO, F. A., PEDROSA-SOARES, A., NEVES, M.A., CALEGARI, S.S., LANA, C. Detrital zircon U–Pb and Lu–Hf constraints on the age, provenance and tectonic setting of arc-related high-grade units of the Araçuaí and Ribeira Orogenic (SE Brazil) transition zone. **Journal of South American Earth Sciences**, v. 116, p. 103861, 2022.

SANTIAGO, R.; CAXITO, F.A.; PEDROSA-SOARES, A.C.; NEVES, M.; DANTAS, E.L.; CALEGARI, S.S.; LANA, C. Records of the accretionary, collisional and post-collisional evolution of western Gondwana in the high-grade core of the Araçuaí-Ribeira Orogenic system, SE Brazil. **Precambrian Research**, v. 397, p. 107191, 2023.

SCHIMIDT-THOMÉ, R. & WEBER-DIEFENBACH, H. Evidence for froze-in magma mixing in Brasiliano calc-alkaline intrusions: the Santa Angélica pluton, southern Espírito Santo, Brazil. **Revista Brasileira Geociências**, v. 17, n. 4, p. 498–506, 1987.

SERRANO, P.; PEDROSA-SOARES, A.; MEDEIROS-JUNIOR, E.; FONTE-BOA, T.; ARAÚJO, C.; DUSSIN, I.; QUEIROGA, G.; LANA, C. A-type Medina batholith and post-collisional anatexis in the Araçuaí Orogeny (SE Brazil). **Lithos**, v. 320–321, p. 515–536, 2018.

SILVA, J.N. DA (Org). Programa levantamentos geológicos básicos do Brasil. **Cachoeiro de Itapemirim. Folha SF.24-V-A-V. Estado do Espírito Santo. Escala 1:100.000**., DNPM/CPRM, 1992.

SKLYAROV, E.V. & FEDEROVSKII, V.S. Magma Mingling: Tectonic and Geodynamic Implications. **Geotectonics**, v. 40, n. 2, p. 120–134, 2006.

SOARES, C.C.V.; QUEIROGA, G.; PEDROSA-SOARES, A.C.; GOUVÊA, L.P.; VALERIANO, C.M.; MELO, M.G.; MARQUES, R.A.; FREITAS, R.D.A. The Ediacaran Rio Doce magmatic arc in the Araçuaí – Ribeira boundary sector, southeast Brazil: lithochemistry and isotopic (Sm–Nd and Sr) signatures. **Journal of South American Earth Sciences**, v. 104, p. 102880, 2020.

SOLLNER, H.S.; LAMMERER, B.; WIEDEMANN-LEONARDOS, C. Dating the Araçuaí Ribeira mobile belt of Brazil. In: Sonderheft, Zeitschrift (Ed.), **Angwandte Geologi**e, SH1, p. 245–255, 2000.

SONG, S.G.; WANG, M.J.; WANG, C.; NIU, Y.L. Magmatism during a continental collision, subduction, exhumation and mountain collapse in collisional Orogenic belts and continental net growth: A perspective. **Science China-Earth Sciences**, v. 58, p. 1284–1304, 2015

SOUSA, C.S.; CONCEIÇÃO, H.; SOARES, H.S.; FERNANDES, D.M.; ROSA, M.L.S. Magmatic processes recorded in plagioclase crystals of the Rio Jacaré Batholith, Sergipano Orogenic System, Northeast Brazil. **Journal of South American Earth Sciences**, v. 118, p. 103942, 2022.

STRECKEISEN, A. To each plutonic rock its proper name. **Earth Sciences Reviews**, v. 12, p. 1–33, 1976.

SUN, S.S. & MCDONOUGH, W.F. Chemical and isotopic systematics of oceanic basalts: implications for mantle composition and processes. In: Saunders, A.D., Norry, M. (Eds.), **Magmatism in Ocean Basins,** Geological Society of London Special Publications, v. 42, p. 313–345, 1989.

TEDESCHI, M.; NOVO, T.; PEDROSA-SOARES, A.C.; DUSSIN, I.; TASSINARI, T.; SILVA, L.C.; GONCALVES, L.; ALKMIM, F.F.; LANA, C.; FIGUEIREDO, C.; DANTAS, E.; MEDEIROS, S.; DE CAMPOS, C.; CORRALES, F.; HEILBRON, M. The Ediacaran Rio Doce magmatic arc revisited (Araçuaí- Ribeira Orogenic System, SE Brazil). **Journal of South American Earth Sciences**, v. 68, p. 167–186, 2016.

TEIXEIRA, W.; SABATÉ, P.; BARBOSA, J.; NOCE, C.M.; CARNEIRO, M.A. Archean and Tectonic Evolution of the São Francisco Craton, Brazil. In: U.G. CORDANI, E.J. MILANI, A. THOMAZ FILHO (Eds) **Tectonic Evolution of South America**, p. 101-137, 2000.

VIEIRA, V.S. & MENEZES, R.G. (Orgs) **Geologia e Recursos Minerais do Estado do Estado do Espírito Santo: texto explicativo do mapa geológico e de recursos minerais, escala 1:400.000.** In: Programa Geologia Do Brasil, CPRM - Serviço Geológico do Brasil, Belo Horizonte, 2015.

WANG, Q.; ZHAO, J.; ZHANG, C.; YU, S.; YE, X.; LIU, X. Paleozoic post-collisional magmatism and high-temperature granulite-facies metamorphism coupling with lithospheric delamination of the East Kunlun Orogenic Belt, NW China. **Geoscience Frontiers** v. 13, p. 101271, 2022.

WHITNEY, D.L. & EVANS, B.W. Abbreviations for names of rock-forming minerals. **American Mineralogist**, v. 95, p. 185–187, 2010.

WIEDEMANN-LEONARDOS, C.M.; MEDEIROS, S.R.; MENDES, J.C.; LUDKA, I.P.; MOURA, J.C. The architecture of late Orogenic plutons in the Araçuaí Ribeira folded belt, southeast Brazil. **Gondwana Research**, v. 5, n. 2, p. 381–399, 2002.

YANG, J.H.; WU, F.Y.; WILDE, S.A.; XIE, L.W.; YANG, Y.H.; LIU, X.M. Tracing magma mixing in granite genesis: in situ U–Pb dating and Hf-isotope analysis of zircons. **Contributions Mineral Petrology**, v. 153, p. 177–190, 2007.

ZHANG, J.; WANG, T.; CASTRO, A.; ZHANG, L.; SHI, X.; THONG, Y.; ZHANG, Z.; GUO, L.; YANG, Q.; IACCHERI, L, M. 2016. Multiple Mixing and Hybridization from Magma Source to Final Emplacement in the Permian Yamatu Pluton, the Northern Alxa Block, China. **Journal of Petrology**, v. 57, n. 5, p. 933–980, 2016.

Submetido em 21 de janeiro de 2025
Aceito para publicação em 15 de abril de 2025